LAND-BASED VECTOR MAGNETIC SURVEY OF BIF-HOSTED IRON ORE

LAND-BASED VECTOR MAGNETIC SURVEY OF A BIF-HOSTED IRON ORE DEPOSIT, MARY RIVER, BAFFIN ISLAND, NUNAVUT

By Ilya Inozemtsev, B.Sc. (Hons)

A Thesis

Submitted to the School of Graduate Studies
In Partial Fulfillment of the Requirements
for the Degree
Master of Science

MASTER OF SCIENCE (2014) McMaster University
(Earth and Environmental Science) Hamilton, Ontario

TITLE: **Land-based vector magnetic survey of a BIF-hosted iron ore deposit, Mary River, Baffin Island, Nunavut**

AUTHOR: Ilya Inozemtsev, B.Sc. (McMaster University)

SUPERVISOR: Dr. Joseph Boyce

NUMBER OF PAGES: ix, 88

Abstract

Banded iron formations (BIFs) are iron oxide- and silica-rich chemical sedimentary rocks and the principal source of high-grade (HG) iron ore. Magnetic survey methods are commonly applied in the exploration for BIF-hosted iron ore deposits but the interpretation of total magnetic intensity (TMI) data is often complicated by the presence of strong remanent magnetization and anisotropy of magnetic susceptibility (AMS). This study evaluated a tri-axial fluxgate vector magnetometer system for ground-based high-resolution mapping of BIF-hosted HG iron ore deposits at a 16 ha site near Mary River, Baffin Island. Magnetometer orientation was measured using a MEMS (Micro Electro-Mechanical System) accelerometer and dual D-GPS receivers. 12-oriented block samples were collected for analysis of rock magnetic properties and supplemented with outcrop measurements using a hand-held susceptibility probe.

The large (3 Gauss) dynamic range of the tri-axial vector magnetometer permitted mapping of HG magnetite ore zones, with TMI in excess of 400,000 nT. A 20 m-wide W-E trending HG zone and a narrow (<10 m) BIF zone were identified in RMV maps with distinctive dipole signatures. Within the HG zone a northwest-southeast oriented magnetic fabric was defined by linear magnetic lows that offset the strike of the HG ore zone and were interpreted as brittle faults or shear zones. The RMV orientation indicated the presence of strong bedding parallel magnetization, while its signal amplitude showed a wide variation between ore types and provided basis for ore grade differentiation. Paleomagnetic measurements revealed high Q ratios for hematite ores and strong AMS for BIF. The results from Mary River demonstrate that remanence and AMS effects are important in BIF-hosted iron ores and cannot be neglected in magnetic interpretation and inversion modelling of magnetic source bodies.

Table of Contents

List of Figures and Tables

Chapter 1

Chapter 2

Acknowledgements

Research work and graduate scholarship were supported by an NSERC Discovery Grant to J. Boyce and a research grant from Baffinland Iron Mines Corporation (BIMC). Logistical and technical support was provided by BIMC over 2013 and 2014 field seasons.

I would like to thank Dr. Joe Boyce for being my supervisor and course instructor for many undergraduate courses, for formulating the concept for this exciting study, for his patience, enthusiasm and continued encouragement.

I would also like to thank Dr. Bill Morris for conducting the paleomagnetic sample analysis and consultations on rock magnetic properties, as well as sharing his tremendous expertise in the field of magnetic geophysics and remote sensing.

I would like to thank my colleagues and fellow students at McMaster University, both undergraduate and graduate, for their friendship, encouragement, and discussions on various topics in Earth Sciences.

Baffinland Iron Mines, and especially Tom Iannelli, Ahoora Samiei, Massoud Robatian and Peter Dao, deserve a very special thank you for the invaluable logistical support that enabled this study to take place in the beautiful and remote Canadian Arctic; and for their enthusiasm, welcoming work environment and encouragement for continuous learning. I would also like to thank my Baffinland colleagues Eli Iannelli, Ludger Makkik, Ryan Ferguson, Jeffrey Wannop and Malte Dehler for assisting with the field survey work and making my field days memorable.

And most of all I would like to thank my parents Slava and Natalia, and my partner Jenna Levi, for the endless love and support that allowed me to continue through my third academic degree experience. All of my most valuable technical skills and abilities, my engineering way of thinking and problem solving, have come from my father and grandfather, who helped open my eyes onto the exciting world of technical and hands on work. For that I am eternally thankful to them.

Chapter 1: Introduction

1. Background

Magnetic survey methods are used widely in mineral exploration for regional-scale resource mapping and for detailed site-scale characterisation of ore deposits (Telford, 1990; Nabighian et al., 2005). Most mineral resource magnetic surveys are conducted using airborne platforms (e.g. fixed-wing or helicopter-borne surveys) but ground-based and borehole magnetic surveys are employed increasingly as a basis for magnetic inversion modelling of ore deposit structure (Mueller et al., 1998; Nabighian et al., 2005; Ugalde et al., 2007).

Iron ore deposits are well-defined targets for magnetic methods as magnetite and hematite-rich ores are readily identified by their large magnetic contrast with host rocks. Aeromagnetic surveys of iron deposits commonly employ magnetic gradiometers or single quantum magnetometers, which measure the scalar intensity (i.e. total magnetic intensity; TMI) or gradient components of the magnetic field. The interpretation of scalar TMI data acquired over iron deposits, however, is often complicated by the presence of strong remanence effects and anisotropy of magnetic susceptibility. Banded iron formations (BIF's) are characteristically magnetically anisotropic sources with high ratios of remanent to induced magnetization ($Q >> 1$) (Clark and Schmidt, 1994) and often with strong anisotropy of magnetic susceptibility. The direction of the remanence vector can differ significantly from the direction of the modern main field as it records the paleomagnetic vector orientation obtained during remanence acquisition. This makes invalid the standard practice of determining the remanence by scalar subtraction of geomagnetic field from the observed total magnetic intensity (Clark, 2014). Determination of the source body magnetization requires measurement of the observed field as a vector, followed by vector subtraction of geomagnetic field given by IGRF (International Geomagnetic Reference Field). Knowing the correct orientation of the source magnetization can simplify interpretation and improve the validity of the inverse

magnetic modelling of the source body. This is particularly true for BIF-hosted iron ore deposits, where magnetic lows can result from a remanence direction that opposes the main field as well as from changes in magnetite content (Dransfield et al., 2003; Wallace, 2007).

1.1 Vector magnetometry

The Earth's magnetic field is a vector quantity (Fig. 1A). The total magnetization vector ($\vec{J}_{total}$) can be represented as the vector sum of the induced and remanent magnetizations (Lelievre and Oldenburg, 2009):

Eq. 1.1
$$\vec{J}_{total} = \vec{J}_{ind} + \vec{J}_{rem}$$

where $\vec{J}_{rem}$ is the remanence and $\vec{J}_{ind}$ is the induction magnetization, which is the product of the Earth's magnetic field $\vec{H}_0$ and magnetic susceptibility χ:

Eq. 1.2
$$\vec{J}_{ind} = \chi\vec{H}_0$$

The induced magnetization is always parallel with the Earth's field, whereas the remanent magnetization vector can have any orientation, as it depends on the field direction during remanence acquisition and the subsequent deformation history of the rock body.

The ratio of remanent to induced magnetization is expressed using the Königsberger ratio (Q), which is the ratio of the magnitudes of remanence and induction vectors:

Eq. 1.3
$$Q = \frac{|\vec{J}_{rem}|}{|\vec{J}_{ind}|} = \frac{|\vec{J}_{rem}|}{|\chi\vec{H}_0|}$$

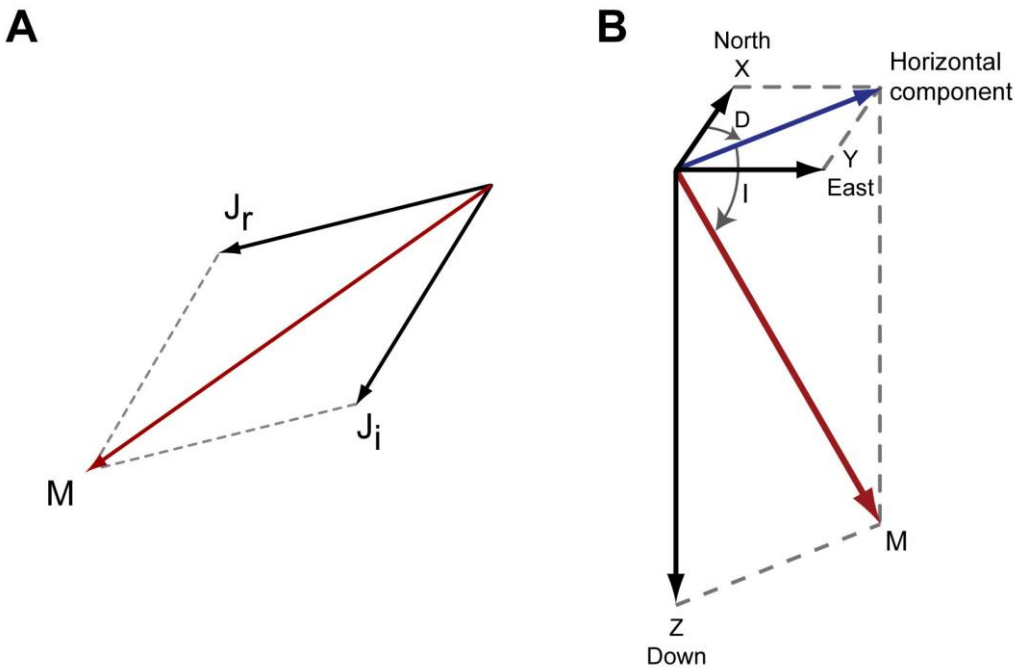

Figure 1. A.) The total magnetic vector J_{total} consists of both an induced component (J_i) due to induced magnetization and a remanence component (J_r). The induction component is oriented in the direction of the main field, whereas the remanence vector records the field direction during remanence acquisition. B). The magnetic vector (M) can be resolved as three mutually perpendicular components (X, Y, Z) within north-east-down (NED) coordinate framework. H is the vector projection in the horizontal (X-Y) plane. The vector orientation is commonly described with respect to the inclination (I) and declination (D) angles. Vector magnetic surveys measure all three magnetic vector components along with its magnitude, while scalar surveys measure only the magnitude of M.

Q is a scalar quantity and is independent of the magnetization directions. Q is typically small in sedimentary rocks (< 0.1) with low magnetite content and Q values of 1-20 are typical for igneous and metamorphic rocks. As shown by Morris et al. (2007), the orientation of the total magnetic vector is highly sensitive to the Q ratio; for values of Q < 0.1, the total magnetization vector approaches the induced magnetization direction and for Q > 10, the magnetization direction is controlled primarily by the remanence component.

Vector magnetometers measure the orientation and magnitude of total magnetic vector, typically by measurement of three mutually perpendicular components (X, Y, Z; Fig. 1). Conventionally, these are measured using the north-east-down (NED) coordinate framework, in which X is positive northward, Y positive eastward and Z positive downwards (Fig. 1B). The total intensity of the magnetic field vector (M) is obtained by vector summation of the components:

Eq. 1.4 $$M = \sqrt{X^2 + Y^2 + Z^2}$$

and the magnitude of the horizontal component (H) is given by:

Eq. 1.5 $$H = \sqrt{X^2 + Y^2}$$

The orientation of the magnetic vector is usually specified using two angles, the vector inclination (I) and declination (D):

Eq. 1.5 $$I = tan^{-1}\left(\frac{Z}{H}\right)$$

Eq. 1.6 $$D = tan^{-1}\left(\frac{Y}{X}\right).$$

Vector magnetic measurements of the Earth's field using magnetometers were first made in the 1930's with the advent of the fluxgate magnetometer (Ripka, 2003). Since that time several types of optically-pumped (quantum) magnetometers and SQUID (super-conducting quantum interference device) magnetometers have been developed for high-precision magnetic vector measurements. Fluxgate magnetometers of various designs are still widely employed for magnetic vector measurements due to their reliability and ease of manufacture. Modern fluxgate magnetometers typically achieve resolutions of about 1 nT with sample rates of up to 1 KHz.

The principle of fluxgate magnetometer operation is shown in Figure 2. A basic fluxgate design consists of two coils wound in opposite directions around a high magnetic permeability ferrite core. An alternating excitation current (I_{exc}) is applied to the inner "drive" coil, saturating the core in alternating directions. The alternating magnetic field produced in the core in turn induces an electrical current in the secondary pick-up coil, which is measured by a sensitive voltmeter. In the absence of an external magnetic field, the flux in one core half cancels the other and the input and output current in the two coils are balanced. In the presence of an external magnetic field (i.e. B_0, Fig. 2), however, the core will become more easily saturated in alignment with the applied field and the output current of the two coils will differ by an amount that is proportion to the external field strength.

Fluxgate magnetometers are used widely for space-borne vector magnetic measurements due to the reliability of solid-state sensors (Ripka, 2003). Their application in exploration geophysics has been somewhat limited to date, as measurements on a moving sensor platform (e.g. airborne survey) require that the sensor orientation be measured to very high levels of accuracy. Measurement of a anomalies to 1 nT resolution for example in a mid-latitude field strength of 55,000 nT requires that the sensor axis orientation is known to about 0.001˚, which is very difficult to achieve without high precision inertial measurement systems. One of the primary applications of fluxgate systems in exploration geophysics to date has been in measurement of aircraft magnetic fields to allow compensation corrections for quantum magnetometer systems. Fluxgate

sensors are also employed as single sensors (i.e. single axis) or in gradiometer configurations for magnetic search applications (e.g. in archaeology, unexploded ordinance detection) where measurements of the magnetic vector orientation are not required. A growing interest in magnetic vector inversion modelling, however, is generating renewed interest in vector magnetometry as a primary field survey method for characterizing the magnetic vector attributes and for identifying the presence of remanence effects (Dransfield et al., 2003; Morris et al., 2007; Ellis et al., 2013).

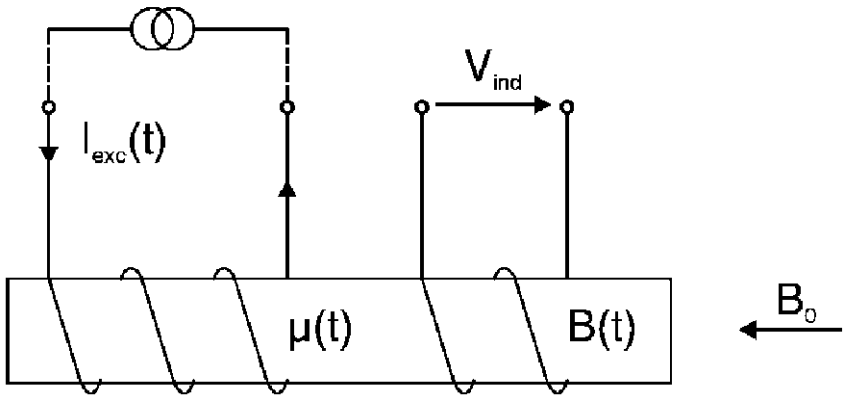

Figure 2. Principle of operation of fluxgate magnetometer (from Ripka, 2003).

1.2 Previous work

Several recent studies have demonstrated the advantages of measurement of the full magnetic vector over scalar magnetic measurements. Dransfield et al. (2003) showed that vector magnetic data routinely acquired by the FALCON airborne gravity gradiometer (AGG) systems could be used to improve airborne mapping of strongly remanently magnetized BIF's in the Marra Mamba Iron Formation, Australia. The attitude data acquired by FALCON inertial sensors were used to correct fluxgate vector magnetometer for platform motions. The magnetic vector data were then enhanced by

calculation of the residual magnetic vector amplitude (see Chapter 2) by subtraction of a regional vector (Christensen and Dransfield, 2002). The subtraction effectively suppresses the magnetic induction component of the vector, producing residual maps that are enhanced in remanence vector components. Isezaski and Matsuo (2009) employed a helicopter-mounted fluxgate magnetometer with attitude data provided by a ring laser gyrocompass capable of measuring the sensor orientation angles with 0.001-degree accuracy. The vector magnetic data was used to better understand the structure of remanently-magnetized volcanic deposits. Although very effective, the above methods are costly to implement and applicable only in airborne surveys already equipped with advanced gyroscopic devices, such as the FALCON gravity gradiometer or a ring-laser gyro. The airborne systems, because of their size and complexity are also not easily adapted to ground-based magnetic survey work.

2. Study Purpose and Objectives

The purpose of this thesis was to evaluate ground-based vector magnetic methods for characterizing BIF-hosted iron ore deposits at the Mary River camp in northwestern Baffin Island (Fig. 3). Baffinland Iron Mines Corporation (BIMC) conducted initial geological mapping in 1965. As part of its exploration program at Mary River further mapping was undertaken during 2009-2013, and drilling at Deposit #4 completed in 2010. Drilling revealed several 15-20 m wide strike-parallel zones containing high-grade magnetite, hematite and specular-hematite (‘specularite’) ores, contained within iron silicate formation and bounded by psammite, quartz-mica schist and gneiss. An airborne magnetic survey of the Mary River district was acquired in 2008, followed by a ground-based magnetic survey of the Deposit #4 in 2010. The ground-based surveys employed potassium (optically-pumped) and Overhauser scalar magnetometers but were unsuccessful in mapping the full extent of high-grade ore deposits due to extremely high field intensity and gradients across the site.

The overall research objective of this study was to evaluate ground-based vector magnetic methods as a geophysical approach for mapping and differentiation of high-grade iron ore deposits. The specific objectives of the thesis were:

1) to develop an integrated fluxgate magnetometer and positioning system for land-based vector magnetic survey under high gradient conditions,
2) to map the extent and geometry of high-grade iron ore deposits at the Mary River Deposit #4 using ground-based vector magnetic methods,
3) to assess the utility of residual magnetic vector intensity (RMVI; Dransfield et al., 2003) and other derived vector magnetic attributes for mapping BIF's and high-grade ore deposits, and for identifying variations in ore grade,
4) to determine the rock magnetic properties of the high-grade ores and BIF host, including the natural remanent magnetization (NRM), anisotropy of magnetic susceptibility (AMS), low-field magnetic susceptibility and Q-ratios.

In order to address the high dynamic range requirements of the survey site, a purpose-built tri-axial magnetometer system was constructed with 3 Gauss (300,000 nT per axis) measurement range. The magnetometer system (described in Section 3.1) consisted of a tri-axial fluxgate magnetometer integrated with a MEMS (Micro Electro-Mechanical System) digital accelerometer and two D-GPS receivers for measurement of sensor attitude.

Figure 3. Location of Mary River mining camp in northwestern Baffin Island, Nunavut, Canada.

3. Methods

3.1 Vector magnetometer system

A major component of this project involved the development and testing of a custom-built vector magnetometer system for ground-based survey of high-grade iron ore deposits. Previous ground-based surveys at Mary River Deposit #4 employing an Overhauser magnetometer measured total magnetic intensities >150,000 nT but were unable to record signals above this amplitude due to the limited gradient tolerance of Overhauser sensors (< 10,000 nT/m). As a result, TMI measurements were obtained over some parts of Deposit #4 but anomaly maxima could not be recorded over high-grade magnetite and hematite ore zones. These zones are of primary economic interest but their continuity and structure could not be determined using the amplitude-limited TMI mapping.

With the requirement for high gradient tolerance and large dynamic range, it was decided that quantum magnetometer would be unsuitable and a custom fluxgate tri-axial magnetometer system was developed (Fig. 4). As no commercial magnetometer system was available, a prototype vector magnetometer was designed using customized sensor components (Fig. 4). The system employed a fluxgate tri-axial magnetometer (Applied Physics model 1540S), a MEMS tilt sensor (OceanServer OS5000) and two D-GPS receivers (ProMark 3) mounted on a 2.7-metre aluminum boom (Fig. 4). The Applied Physics 1540S fluxgate was selected based on its wide dynamic range, which could be further increased at the factory to ±300,000 nT (± 3 Gauss) per axis, making it suitable to measure the full range of magnetic field observed at the site (> 400,000 nT). The 1540S sensor is a fully digital fluxgate sensor incorporating 24-bit Sigma-Delta analog to digital converter with noise level of <5 microGauss (0.5 nT peak to peak) and an absolute accuracy of 1 nT. The fluxgate is designed with a high precision sensor mounting blocks with an axis orthogonality $\leq \pm 0.2^{\circ}$. The sensor is powered by a 9-volt external power supply and uses a RS-232 protocol for data transmission to a serial port.

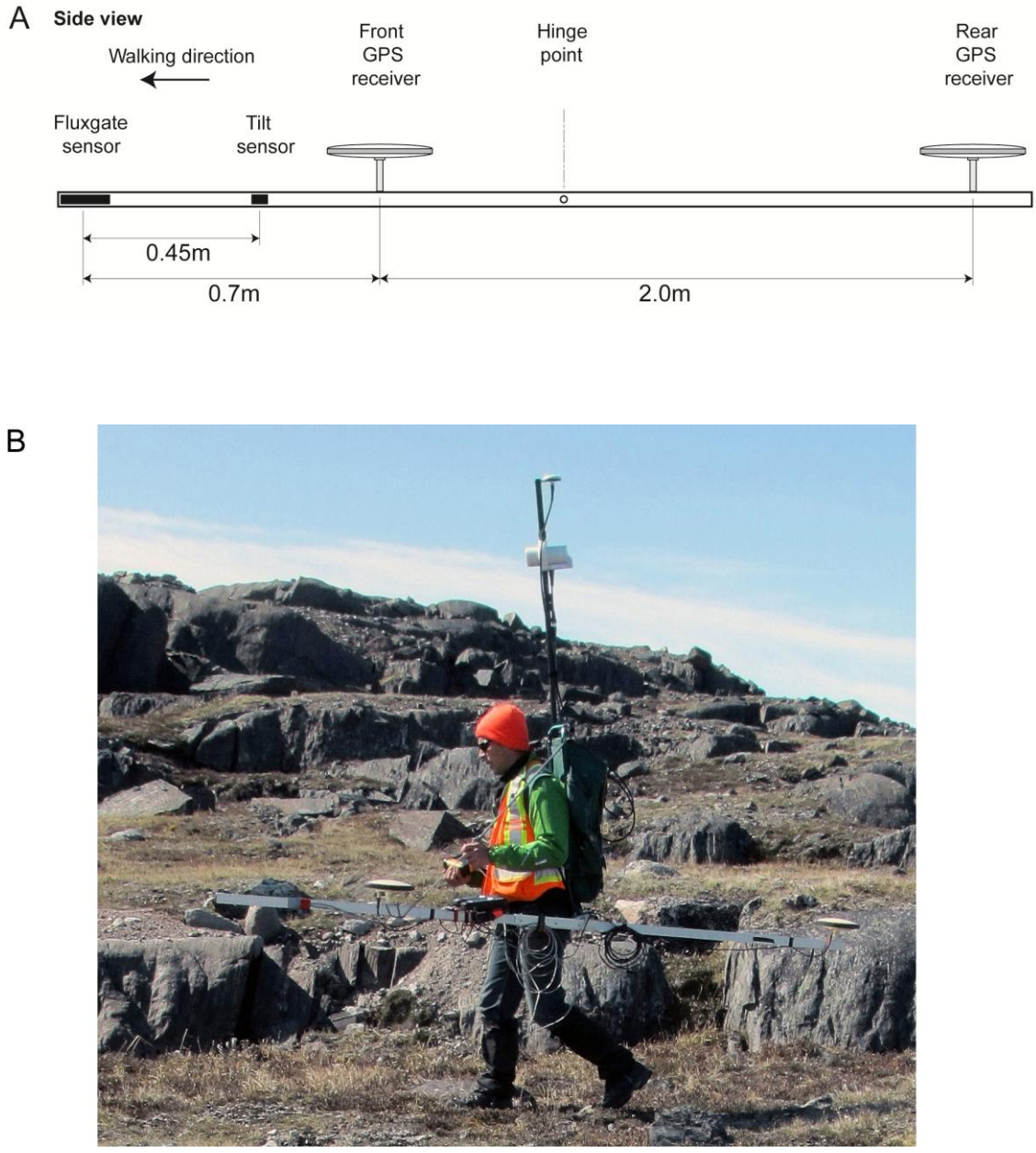

Figure 4. A) Prototype vector magnetometer system, consisting of a single fluxgate tri-axial magnetometer (Applied Physics 1540S) mounted on the end of a 2.7 m aluminum boom. A MEMS tilt sensor (OceanServer OS5000) and two D-GPS receivers (ProMark 3) also mounted on the boom recorded sensor pitch, roll and yaw (azimuth).
B) Fluxgate system in use during a ground-based survey of Deposit #4 at Mary River. A second Overhauser magnetometer (GEM GSM-19) was pole-mounted on the backpack and used to record the absolute total magnetic intensity (TMI).

One drawback of all fluxgate magnetometers is that their readings are subject to a time and temperature dependent drift, which must be compensated in order to produce reliable vector component and total field readings (Ripka et al., 2003). The Applied Physics 1540S has a specified temperature-dependent drift of <1 nT/°C, which was confirmed during testing and found to be generally linear and repeatable. In order to compensate for fluxgate sensor drift, an Overhauser sensor was incorporated into the magnetometer system to allow absolute measurement of the total field magnetic intensity over the low-field (typically < 150,000 nT) areas of the field site. The TMI readings provided by the Overhauser sensor were used to monitor fluxgate drift and to verify the TMI calculated from the tri-axial magnetic components.

The sensor boom pitch and roll angles were measured using the OceanServer OS5000 digital compass (Fig. 4). The compass employs a 3-axis anisotropic magneto-resistance sensor (AMS) magnetometer and a 3-axis micro-electro-mechanical systems (MEMS) accelerometer to measure pitch and roll with an accuracy of 1^{o} and yaw (azimuth) with accuracy of 0.5^{o} (RMS) (OceanServer Technology Inc., 2010). Due to the high magnetic field intensity at Deposit #4, the yaw values provided by the AMS compass were unreliable and instead the sensor azimuth was measured using two ProMark3 D-GPS receivers mounted at a 2 m separation on an aluminum boom (Fig. 4). The differential positions provided by the D-GPS receivers had a post-processed error of ±0.05m, providing azimuth (sensor yaw) measurements with an estimated accuracy of ±1.5º. The fluxgate magnetometer and tilt sensor data were logged on a Trimble Yuma™ ruggedized field computer using RS-232 interface. The data streams were synched using UTC reference time provided by the D-GPS.

In order to evaluate potential magnetic interference between the sensor components, tests were performed to determine the separation distance of the MEMS sensor and D-GPS receivers from the fluxgate magnetometer. The test results are provided in Appendix 1. The optimum sensor-magnetometer offset distance was determined by varying the separation of each sensor from the fluxgate magnetometer in a low field area and observing the change in the total magnetic field intensity. The

Promark3 receivers were found to have the largest interference effect on the fluxgate sensor due to a ferrite core within the receiver. Positioning of the D-GPS receiver 0.7 m from fluxgate sensor resulted in a magnetic anomaly of < 35 nT, which was deemed acceptable given the large magnitude of anomalies present at Deposit #4. Locating the MEMS tilt sensor 0.45 m from the fluxgate resulted in < 1 nT anomaly. Interference between the Yuma tablet computer and fluxgate sensor was negligible (< 1 nT) at a distance of 1 m or greater (see Appendix 1 for test results).

3.2 Field survey methods

In order to field test and evaluate the magnetometer system, a detailed ground-based vector and total magnetic survey was conducted over a 400 x 400 m (0.25-km^2) test site at the Deposit #4 at Mary River (Fig. 3). The survey was conducted as part of a collaborative research project between McMaster University and Baffinland Iron Mines Corporation (BIMC). A total of 11-line km of magnetic survey data were acquired using the tri-axial vector magnetometer system. The survey contained 21 lines oriented N-S, and spaced 20m, as well as 7 E-W tie lines at 50 m intervals. In order to validate the walking survey results, static point measurements of the magnetic vector were collected along a single line (Line 5) of the survey grid. For static measurements the fluxgate sensor was mounted on a non-magnetic tripod and carefully levelled at each station. Static magnetic vector measurement readings were collected at 3 m spacing across the main ore body and at 10 m intervals on the host rock areas. Each tri-axial field measurement was followed by careful D-GPS (Trimble^{TM} R8) measurement of the fluxgate azimuth using the same computation method outlined for the walking survey.

3.3 Data Processing

The project data consisted of four data sets that were acquired separately, and subsequently merged into a single database (Fig. 5). These included Overhauser TMI data, fluxgate tri-axial data (X, Y, Z components), MEMS tilt data and D-GPS positional data. All four data sets were processed in Geosoft Oasis Montaj software using the processing flow summarized in Figure 5. The processing of the magnetic vector data employed a conventional aeromagnetic processing flow (Luyendyk, 1997; Pozza et al. 2004), and included removal of spurious signal and drop-outs, followed by lag and diurnal corrections. An additional filtering step involved phase-aligning the X,Y and Z components of the fluxgate signal. The Applied Physics logging software records data at an average rate of 52 Hz, but uses 4 rows in the output file for each tri-axial reading of the magnetic field: values of X, Y and Z are recorded one per row, followed by TMI value, thus resulting in the effective sampling rate of 13 Hz.

The high-amplitude short-wavelength signal of the MEMS tilt sensor was smoothed using a 5-sample low-pass filter LOWPASS routine in Geosoft Oasis Montaj (Fraser, 1966). The Overhauser and ProMark3 GPS data sets did not require any signal filtering. Diurnal corrections were applied using TMI measurements continuously recorded at base-station Overhauser magnetometer located in a low gradient area 20 km to the south of the survey site.

Processing of D-GPS data involved differential baseline processing in ProMark3 GNSS Solutions software, followed by sensor boom azimuth computation in Geosoft Oasis Montaj. The sensor azimuth was computed using a trigonometric relationship (Eq. 1.7) defining the declination angle α in terms of difference in the Easting (Δx) and Northing (Δy) between two GPS receivers (Fig.4). The result was then corrected for the correct compass quadrant to convert the angle to 360-degree azimuth scale.

Eq. 1.7
$$\alpha = \tan^{-1}\frac{\Delta x}{\Delta y}$$

Clock synchronization of data streams presented the largest challenge, as the fluxgate sensor, MEMS accelerometer and D-GPS operated with independent clocks. Transmission of fluxgate magnetometer data to the RS-232 serial port resulted in a latency in magnetometer readings of up to 5 sec. The time lag was corrected by comparing the profiles of common channels shared by some data sets. Both magnetometers and the MEMS sensor shared a total magnetic intensity channel, allowing the time offset between data sets to be determined by alignment of selected well-defined anomalies on TMI profiles. A similar approach was used to synchronize the GPS position channels of the D-GPS and the Overhauser data sets, by aligning their respective coordinate profiles. Time lags determined this way were applied to the clock channels of each data set, resulting in a fully time-synchronous database.

The sensor pitch, roll and azimuth angles (Tait-Bryan angles) recorded by the magnetometer system were used in post-processing to correct the magnetic vector components for sensor orientation and to bring all vector measurements to a common geographic reference framework. This correction was applied through a matrix rotation operation (Equation 1.8) that converted attitude angles measured in a moving reference frame M to those in a fixed or inertial reference frame I (LaValle, 2006). The coordinate system employed corresponded to the NED (North-East-Down) configuration, with the positive X-axis pointing in the direction of survey travel, positive Y-axis pointing to the right, and positive Z-axis pointing down (Fig. 1). The sign convention for attitude angles was as follows: the angle of rotation around a given axis is considered positive in the clock-wise direction, when looking in the positive direction of the axis. The matrix rotation was performed on the X, Y and Z vector components using the operator in Eq.1.8.

Eq. 1.8

$$R_I^M(y,p,r) = \begin{pmatrix} cos(y)cos(p) & cos(y)sin(r)sin(p) - cos(r)sin(y) & sin(r)sin(y) + cos(r)cos(y)sin(p) \\ cos(p)sin(y) & cos(r)cos(y) + sin(r)sin(y)sin(p) & cos(r)sin(y)sin(p) - cos(y)sin(r) \\ -sin(p) & cos(p)sin(r) & cos(r)cos(p) \end{pmatrix}$$

where *y* is the yaw, *p* is the pitch and *r* the roll angles in degrees.

Following the attitude corrections, the individual X, Y and Z components were gridded using a minimum curvature algorithm (Briggs, 1974) with a grid cell size of 5 m. The total magnetic intensity (TMI) was calculated from the individual vector components by vector summation. The gridded individual X, Y and Z components (see Chapter 2) displayed considerable line-to-line corrugation. The TMI grid calculated from the X, Y and Z magnetic components, however, showed little corrugation, indicating that the issue was not the sensor calibration but imperfect attitude corrections due to inaccuracies in pitch, roll and yaw measurements. As described by Schmidt et.al. (1993) vector magnetic surveys are extremely sensitive to the sensor orientation, necessitating measurement of angles to about 0.001 degree in order to achieve an accuracy of 1 nT in a field of 55, 000 nT . For the purpose of analysis of individual vector component maps, each component was levelled using careful line-by-line tilt-levelling using two synthetic dummy ties located at the northern and southern ends of the survey area. These ties were produced by fitting a polynomial to their intersection miss-ties with survey lines.

Following levelling the residual magnetic vector intensity (RMVI) and residual inclination and declination (D_{RMV}, I_{RMV}) were computed by vector subtraction according to the method of Christensen and Dransfield (2002) using of the regional vector calculated using an IGRF (International Geomagnetic Reference Field) model for the Mary River. Details of the residual vector subtraction methods are explained in detail in Chapter 2.

The Analytic Signal Amplitude (ASA) was computed using the three mutually-orthogonal gradients of the TMI, as shown in Eq. 1.9 (Nabighian, 1972), where T is the total magnetic intensity at location (x,y), and A(x,y) is the amplitude of the analytic signal.

Eq. 1.9 $$|A(x,y)| = \sqrt{\left(\frac{dT}{dx}\right)^2 + \left(\frac{dT}{dy}\right)^2 + \left(\frac{dT}{dz}\right)^2}$$

In final step, the residual vector attributes and ASA were interpolated with 5 m grid cell size using minimum curvature gridding (Briggs, 1974) and displayed as colour-shaded images.

3.4 Rock magnetic property analysis

12 oriented block samples were collected at Deposit #4 for measurement of rock magnetic properties. Oriented block were sub-sampled using a 1.5 cm diamond-coring bit and the natural remanent magnetization (NRM) measured using a Molspin magnetometer, AF demagnetizer and pulse magnetizing system. The low-field susceptibility (κ) and anisotropy of magnetic susceptibility (AMS) were measured on a Bartington MS-2B susceptibility meter. Rock magnetic property analyses were conducted by Dr. Bill Morris in the Applied Geophysics Lab at McMaster University.

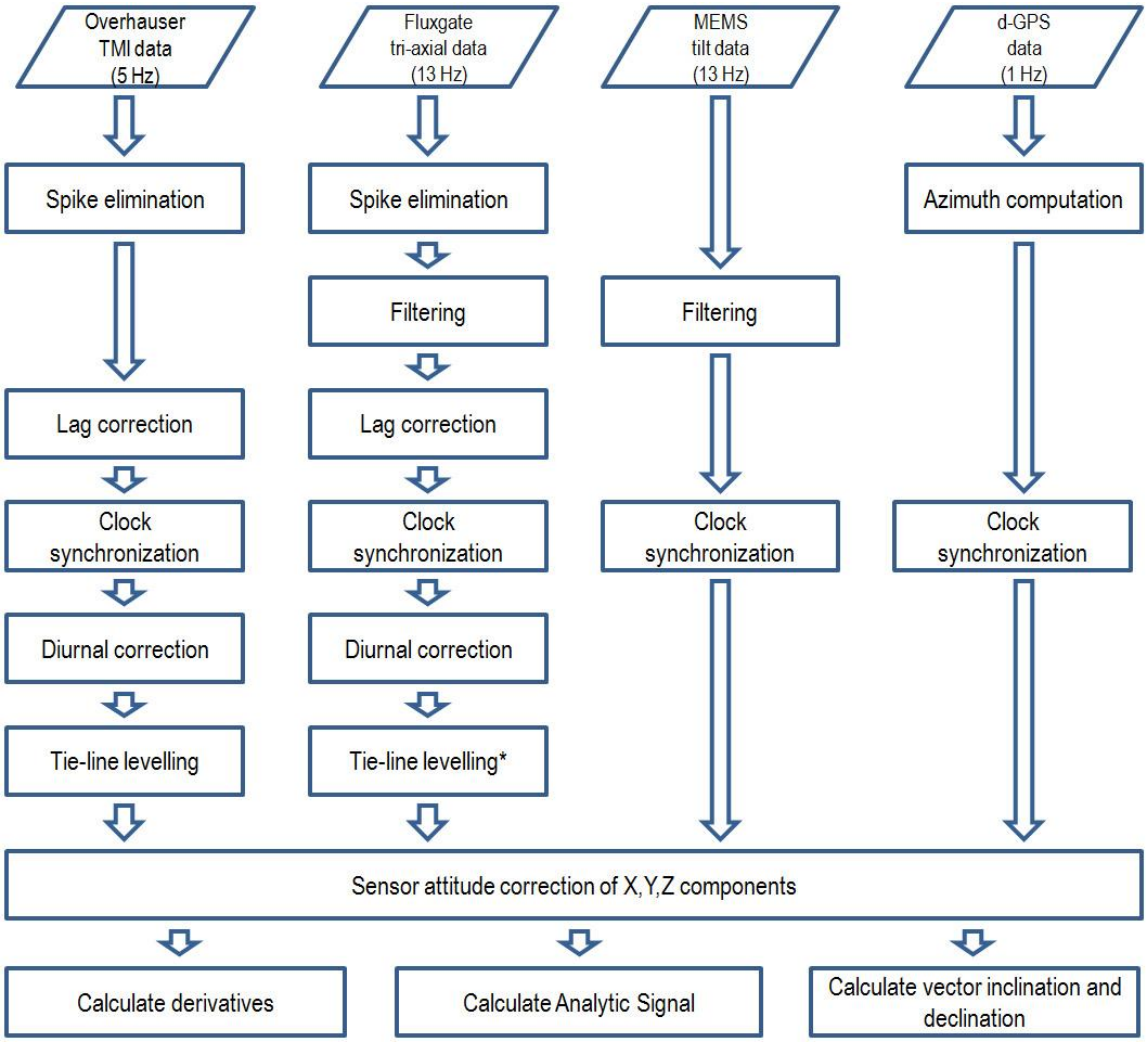

Figure 5. Schematic processing flow showing steps in integration of magnetometer, MEMS tilt meter and D-GPS data sets. A modified aeromagnetic processing flow (Luyendyk, 1997; Pozza et al. 2004) was used for magnetic data.

4. Statement on Authorship

Chapter Two will be submitted in revised form for publication in *Exploration Geophysics*. Contributions to the research are outlined here as required by the School of Graduate Studies. I. Inozemtsev was responsible for survey instrument design and assembly, survey data collection, processing and analysis, as well as preparation of all figures. J. Boyce supervised the thesis research, including project conception, instrument and survey design, interpretation of results and editing and preparation of manuscript. Several valuable geological maps and diagrams were provided by Thomas Iannelli of Baffinland Iron Mines. Peter Dao and Ludger Makkik (Baffinland) assisted with field data collection. Jeffrey Wannop and Eli Iannelli (Baffinland) assisted with rock sample collection. Paleomagnetic sample preparation and magnetic rock property analyses were conducted in the McMaster University Applied Geophysics lab by Dr. Bill Morris.

Chapter 2: An Evaluation of Ground-based Vector Magnetic Surveys for Mapping of BIF-hosted Iron Ore Deposits at the Mary River Camp, (Baffin Island, Canada)

Abstract

The interpretation of magnetic total field data acquired over high-grade iron ore deposits is often complicated by the presence of strong remanent magnetization and anisotropy of magnetic susceptibility (AMS). In this study, we evaluated a tri-axial fluxgate vector magnetometer system for ground-based high-resolution mapping of BIF-hosted high-grade iron ore deposits at a 16 ha site near Mary River, Baffin Island. The magnetometer orientation was measured using MEMS (Micro Electro-Mechanical System) accelerometer and dual D-GPS receivers mounted on a 2.7-m aluminum boom. A second Overhauser magnetometer was employed to measure the absolute total magnetic intensity (TMI). Static magnetic vector measurements were acquired along a single survey for comparison with the walking magnetometer survey. The residual magnetic vector (RMV) intensity, declination and inclination were calculated by subtraction of a constant regional vector (declination 36.6°W, inclination 85.4°). 12-oriented block samples of BIF, high-grade iron ore and host rock were collected for analysis of rock magnetic properties (natural remanent magnetism, AMS, magnetic susceptibility, density) and were supplemented with outcrop magnetic susceptibility measurements using a hand-held probe.

The large dynamic range of the tri-axial vector magnetometer system permitted mapping of high-grade magnetite ore zones, where the total field intensity was in excess of 400,000 nT. High-grade ore zones were identified in RMVI maps by a 15-20 m wide W-E trending zone of high magnetic intensity with a distinctive dipole signature. Within the ore zone a northwest-southeast oriented magnetic fabric was defined by linear magnetic lows. Lineaments offset the strike of the main high-grade ore zone with an apparent sinistral displacement and are interpreted as brittle faults or shear zones. RMV

mapping also revealed a narrow (< 10 m) 200 m long zone of BIF paralleling the main high-grade ore zone. The orientation of the residual magnetic vector indicates the presence of strong bedding parallel magnetization but the residual inclination and declination were not diagnostic of high-grade ore types. The RMV signal amplitude and peak intensity showed a wide range of variation between ore types and provided basis for differentiation of ore grades; high-grade magnetite ores had a mean RMV intensity ~195,000 nT (maximum > 360,000 nT), specularite-hematite ~90,000 nT (maximum > 230,000 nT) and BIF ~52,000 nT (maximum > 68,000 nT). Paleomagnetic measurements revealed high Q ratios for coarse magnetite (5.2) and specular hematite ores (30-107) in comparison with host BIFs (0.1-0.2). The ores have a high degree of anisotropy (AMS > 1.25), indicating a strong layer parallel magnetization of BIF's and ore deposits. The results from Mary River demonstrate that remanence and anisotropy effects are important in BIF-hosted iron ores and cannot be neglected in magnetic interpretation and inversion modelling of magnetic source bodies.

Keywords: Ground-based vector magnetic survey, fluxgate magnetometer, iron ore deposit

1. Introduction

Scalar measurements of the total magnetic intensity (TMI) are used widely for ore deposit mapping and inversion modelling of source body geometry and depth (Nabighian et al., 2005; Wallace, 2006; Morris et al., 2007; Ellis et al., 2013). TMI measurements, however, provide little information about the orientation of the magnetic field vector or the presence of remanent magnetization. As a consequence, the interpretation TMI data often relies on the assumption that magnetic induction is the primary source of magnetization (i.e. Q < 1)(Morris et al., 2007; Lelièvre and Oldenburg, 2009). Such assumptions are invalid when magnetic source bodies are strongly remanently

magnetized (Q >> 1) in a direction that is different from the main field, and as a result, TMI anomaly patterns can be complex and difficult to interpret (Dransfield et al., 2003; Morris et al., 2007).

The interpretation of TMI anomalies in banded iron formations (BIF's) can be particularly challenging, as they are often strongly remanently magnetized with an anisotropy of magnetic susceptibility (AMS) that can be up to four times greater in the direction parallel with bedding (Clark and Schmidt, 1994; Guo et al., 2011; Clark, 2013). Where strong AMS is present, self-demagnetization effects within thin, high susceptibility (> 0.1 SI) layers can also contribute to anomalous changes in magnetic intensity, as they tend to deflect the magnetic vector in the direction of bedding (Guo et al., 1998; Wallace, 2007; Austin et al., 2014). Remanence magnetization in BIF's often shows a strong preferred orientation due to anisotropic remanence acquisition and is typically acquired more readily along the bedding than across it. According to Guo et al. (1998), remanence anisotropy in BIF's generally exceeds the AMS, and can lead to significant deflection of the total magnetic vector from the true paleomagnetic direction, particularly for remanences acquired at high latitudes. The net effect of AMS and anisotropy of remanence acquisition is that the total magnetization vector in BIF's tends to be strongly deflected towards the bedding plane orientation and complex magnetization patterns may arise when layers have undergone folding and refolding, as is the case in many polydeformed Archean greenstone belts.

The presence of remanence and AMS effects need to be considered when interpreting TMI data, as they can mimic magnetic anomalies produced by zones of alteration and mineralization in BIF's (Clark and Schmidt, 1994; Wallace, 2007). The enrichment of BIF to iron ore, for example, is commonly associated with the alteration of magnetite to hematite and an corresponding decrease in TMI due to the reduction in magnetic susceptibility (Kerr, 1994; Gunn and Dentith, 1997; Hagemann et al., 2007). However, anomalous TMI lows can also be produced by a remanence that opposes the main field vector or due to self-demagnetization of thin layers in BIF's (Wallace, 2007). Conversely, in cases where the remanence vector is aligned with and reinforces the main

field vector, the TMI will be locally increased, and can be misinterpreted as an increase in induced magnetization and magnetic susceptibility. A case can also exist where the remanence vector is of equal magnitude and opposite to the direction of induction magnetization and no measurable TMI anomaly is generated (Morris et al., 2007). In all cases, if TMI anomalies are attributed to changes in induction magnetization alone, the magnetic interpretation and source characteristics estimated through inversion modelling will be subject to large uncertainties and possibly errors (Lelièvre and Oldenburg, 2009; Paine et al., 2012; Ellis et al. 2012; Pilkington and Beiki, 2013).

An alternative approach that can assist in magnetic interpretation of remanently magnetized iron ore deposits is to directly measure the magnetic vector orientation and magnitude using vector magnetic surveys (e.g. Ladynin et al., 2002; Christensen and Dransfield, 2002) or paleomagnetic studies (Morris et al., 2007). Vector magnetometers (e.g. fluxgate sensors) measure both the orientation and magnitude of the Earth's magnetic field using three mutually orthogonal sensors. The magnetic vector components are measured relative to a geographic reference framework and used to calculate the declination, inclination and magnitude (intensity) of the total magnetic field vector (Fig. 1). Where strong remanence effects are present in ore bodies, deviations of the measured magnetic vector from the modern main field direction can provide a rapid indicator of the presence of remanence and self-demagnetization effects. Christensen and Dransfield (2002) employed fluxgate vector magnetic measurements collected as part of FALCON airborne gravity surveys to map and interpret remanence effects in BIF's of the Hamersley Basin in Australia. The attitude data acquired by FALCON inertial sensors were used to correct fluxgate sensor motions and the vector data were further enhanced by subtraction of a constant regional (e.g. IGRF) vector. The vector subtraction yields what is known as the residual magnetic vector (RMV) amplitude:

Eq. 2.1
$$RMV = \begin{bmatrix} X_{res} \\ Y_{res} \\ Z_{res} \end{bmatrix} = \begin{bmatrix} X_{obs} \\ Y_{obs} \\ Z_{obs} \end{bmatrix} - \begin{bmatrix} X_{IGRF} \\ Y_{IGRF} \\ Z_{IGRF} \end{bmatrix}$$

where X_{res}, Y_{res} and Z_{res} are the RMV residual components in the x (east), y (north) and z (down) directions, X_{obs}, Y_{obs} and Z_{obs} are the measured vector components and X_{IGRF}, Y_{IGRF} and Z_{IGRF} the regional vector components obtained from IGRF (International Geomagnetic Reference Field) model or determined by field measurement (Fig. 1). As an alternate method, the average value of the vector components across the entire survey area can be used an approximation of the regional vector for subtraction (Christensen and Dransfield, 2002).

Several other useful magnetic attributes can also be derived from the fully corrected RMV components, including the horizontal component of the RMV:

Eq. 2.2 $$H_{RMV} = \sqrt{{X_{res}}^2 + {Y_{res}}^2}$$

the residual magnetic vector declination:

Eq. 2.3 $$D_{RMV} = tan^{-1}\left(\frac{Z_{res}}{H_{res}}\right)$$

the magnetic vector inclination:

Eq. 2.4 $$I_{RMV} = tan^{-1}\left(\frac{X_{res}}{Y_{res}}\right)$$

and the residual magnetic vector intensity (amplitude) (Fig. 1B):

Eq. 2.5 $$RMVI = \sqrt{{X_{res}}^2 + {Y_{res}}^2 + {Z_{res}}^2}$$

In contrast with the Earth's main field vector, which is relatively invariant over regional scales, the inclination and declination of the RMV can vary through a full range

of angles (Dransfield et al., 2003). Mapping of the variations in the RMVI and its orientation (i.e. I_{RMV}, D_{RMV}) across a survey area can rapidly highlight deviations in the magnetic vector from the orientation of the main field vector (Ladynin et al., 2002)(Fig. 1B). When combined with conventional TMI measurements, the RMVI and derived attributes provide an effective means of characterizing the relative importance of induced and remanence components of magnetization and can provide improved input data for modelling of source body depths and geometries (Paine et al., 2012). It is important to note that RMVI and its inclination and declination (I_{RMV}, D_{RMV}) do not directly yield the remanence vector (Fig. 1) but in areas where Q is large (i.e. > 10; Morris et al., 2007) the orientation of residual vector will approach the remanence vector direction.

Vector magnetic methods have many advantages over TMI measurements but are rarely employed in resource exploration due to the requirement for high-precision positional and attitudinal data (Schmidt et al., 1994). As an example, the measurement of a TMI anomaly with a resolution of 1 nT in a field strength of 55,000 nT requires that the sensor orientations be measured with an accuracy of about 0.001 degree. This level of positional accuracy has been difficult to achieve without expensive inertial navigation systems but the recent availability of more precise inertial navigation technology (e.g. optical gyros) and low-cost MEMS (micro electro-mechanical systems) accelerometers has made it more economical and feasible to collect vector magnetic data from moving sensor platforms (e.g. aircraft, walking surveys). In one of the few recent published studies, Dransfield et al. (2003) demonstrated the successful application of vector magnetics acquired with the FALCON system for mapping iron mineralization in the Hamersley Group BIF in western Australia. The Hamersley BIF is contained within a broad synclinal structure with fold limbs that show a marked difference in TMI, which could not be reconciled with the mapped ore deposit geology. The RMV maps produced in that study more closely matched the mapped geology confirming that variations in intensity along the fold structures was due to a strong remanent magnetization. The remanence directions measured by the vector magnetometer survey matched closely those obtained by rock property measurements (Clark and Schmidt, 1994), confirming

that in-situ measurement of effective remanence direction is feasible with airborne vector magnetic methods.

In this paper we report on the results of a ground-based vector magnetometer survey of BIF-hosted high-grade iron ore deposits at the Mary River mining camp in northwestern Baffin Island, Nunavut, Canada (Fig. 2). The Mary River BIF's, like the Hamersley Group, are highly magnetized and characterized by complexly folded TMI anomaly patterns and large dipolar anomalies (-20,000 to > 300,000 nT) which have complicated the acquisition and interpretation of TMI data. The large variation in the TMI values at Mary River can be attributed in part to the spatial variations in the concentrations of enriched magnetite and hematite ore bodies within the BIF, but also points to the presence of an unquantified component of remanent magnetization.

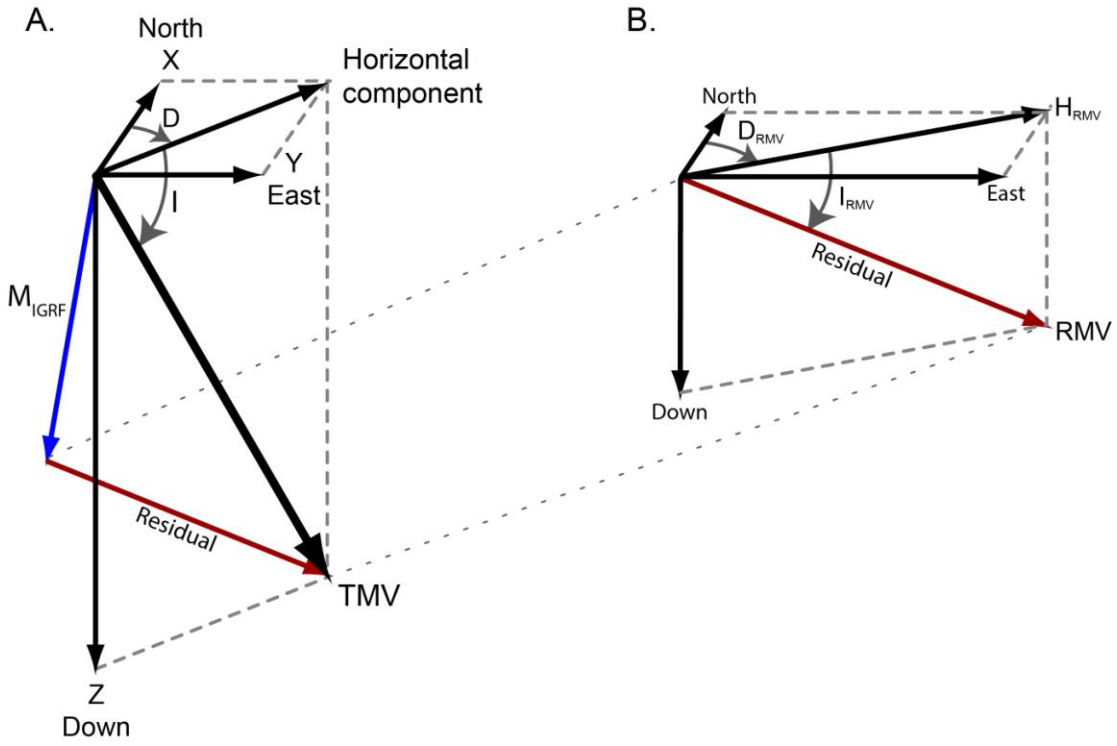

Figure 1. A. The total magnetic vector (TMV) is commonly measured using a tri-axial magnetometer as three orthogonal magnetic components within a north-east-down (NED) coordinate framework. B. The residual magnetic vector (RMV) is calculated by subtraction of a regional magnetic vector (M_{IGRF}), which approximates the main field (induction) vector. The deflection of the RMV from the regional vector orientation indicates the presence of significant remanence or other components of magnetization (e.g. self-demagnetization), which are unrelated to induction (after Christensen and Dransfield, 2002).

Complex anomaly patterns likely also result from the strong anisotropy of the magnetic susceptibility and remanence in the BIF, particularly where the bedding orientation changes occur due to folding (Morris et al., 2007). These knowledge gaps highlighted the need for more detailed study of the magnetic properties of Mary River iron ores and BIF host rocks in order to develop improved magnetic field survey methods and to better resolve interpretations and geological models.

Previous airborne and ground-based TMI surveys at Mary River were conducted using potassium (optically-pumped) and Overhauser scalar magnetometers but were unsuccessful in mapping the full extent of high-grade ore deposits due to extremely high magnetic gradients across the site. In this study we evaluated a new tri-axial fluxgate magnetometer system, which integrates a MEMS (Micro Electro-Mechanical System) digital accelerometer and D-GPS receivers for recording and post-survey correction of sensor attitudes. Our results demonstrate that high-grade magnetite and hematite ore zones can be distinguished from BIF and psammite host rocks on the basis of the residual magnetic vector amplitude (intensity) and systematic changes in the vector orientation. High-resolution mapping of the TMI and residual magnetic vector intensity (RMVI) yielded important new information regarding the continuity and structure high-grade ore zones, including the presence of previously unrecognized system of faults that offset the strike of the ore deposits. This study represents the first successful application of ground-based vector magnetic survey for mapping and characterizing BIF-hosted high-grade iron ore deposits at Mary River. The results and methods reported here can be applied more broadly elsewhere in exploration of iron ore deposits and are amenable to high magnetic gradient environments where remanence effects are likely to complicate the acquisition and interpretation of TMI data using conventional scalar magnetometers.

2. Study Area and Geologic Setting

Ground-based vector magnetic surveys were conducted over a 16 ha site (Fig. 2) at the Baffinland Iron Mines Corporation (BIMC) Deposit #4 property, located 25 km northwest of Mary River, in northwestern Baffin Island (Fig. 2). Exploration in the Mary River district began in the early 1960's and during the last decade BIMC has conducted a detailed program of geological mapping, airborne and land-based geophysics and diamond drilling. Several sizable high-grade iron deposits have been discovered at Mary River, including Deposit #1, which contains an estimated 365 Mt of direct shipping ore (DSO) with an average iron grade of 65 wt % Fe. In 2014, BIMC began developing an open pit mine at Deposit 1 with a planned production of 18 Mt per year.

Mary River lies within the 3.0-2.5 Ga Committee Bay Belt (CBB) of the eastern Churchill Province (Fig. 2), comprising an assemblage of greenschist to upper-amphibolite-facies supracrustal rocks and rift basin volcanics and metasediments overlying Mesoarchean basement (Jackson and Berman, 2000). High-grade iron ore deposits are hosted within Archean (2.76 – 2.71 Ga) Algoma-type banded iron formations of the Mary River Group (Young et al., 2004; Johns and Young, 2006; MacLeod, 2012). The Mary River Group consists of sequence of mafic to intermediate volcanics and banded-iron formation, overlain by felsic volcanics and greywackes. Iron ore enrichment of BIF at Mary River has been attributed to a multi-phase process, involving the formation of dome and keel structures during the Trans-Hudson Orogeny (2.0-1.8 Ga) with subsequent desilication, leaching and thermal metamorphism, yielding high-grade ores composed of magnetite, specular hematite, martite, as well as residual banded iron ore (MacLeod, 2012). MRG iron ore deposits are exposed along the Central Borden Fault (Figs. 2, 3) and in fold structures that form topographic ridges up to 700 m in height. In other areas, ore deposits are covered by a variable thickness of Pleistocene overburden and Paleozoic carbonate rocks.

The Deposit #4 study site is located on the north limb of the McOuat synform (Fig. 3), an eastward plunging fold structure cored by Mary River Group metasediments, BIF and minor amphibolites (MacLeod, 2012). The synform is bounded to the north and south by mylonitic detachment faults and in the west by the Central Borden Fault (CBF) (Fig. 3). High-grade iron deposits form west-east striking elongated lenses and zones up to 70 m in width (Fig. 3). High-grade ores are comprised dominantly of magnetite with localized bands up to 15-20 thick of specular hematite hosted in BIF or silicate iron formation. The subsurface geometry of the iron ore deposits is not well constrained borehole data are limited (Fig. 4). Geological models based on existing borehole data have interpreted the high-grade ores and host BIF units as planar tabular units that dip at high angle (~ 85º) to the south towards the axis of McOuat syncline (Fig. 5).

Previous magnetic survey work at Deposit #4 has included ground-based and airborne (heli-mag) TMI surveys to map the extent of high-grade ore deposits. The heli-mag data (Fig. 6) clearly show the synclinal fold structure, with high intensity areas corresponding with high-grade magnetite and hematite ores and BIF host rocks. The along strike continuity of the BIF and high-grade ores appears to offset locally by faulting or secondary folds, but the airborne data provide insufficient resolution for detailed structural mapping. Ground-based TMI surveys were conducted at Mary River in 2010 using a single Overhauser magnetometer with the aim of mapping the high-grade ore deposit contacts and structure in detail. The surveys measured total magnetic intensities up to 130,000 nT across high-grade ore zones but were unable to record larger amplitudes due the limited gradient tolerance of Overhauser sensors (< 10,000 nT/m). As a result, TMI measurements were obtained over about 80% of Deposit #4 but anomaly maxima could not be recorded over high-grade magnetite and hematite ore zones. These zones are of primary economic interest to but their continuity and structure could not be determined using the amplitude-limited TMI maps.

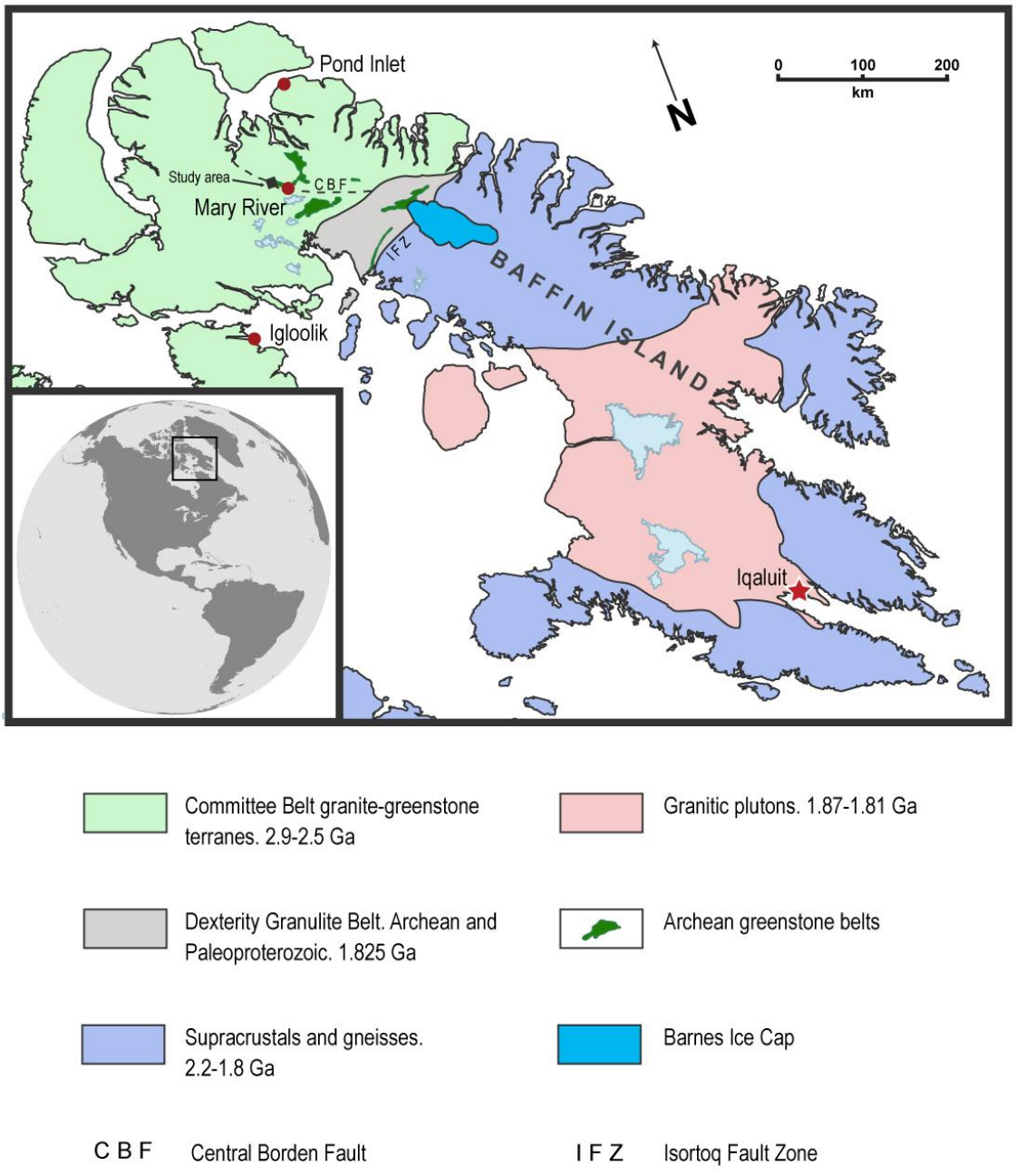

Figure 2. Location of Mary River mining camp in northwestern Baffin Island, Nunavut, Canada. Regional scale bedrock geology is shown (modified from Johns and Young, 2006; Jackson and Berman, 2000).

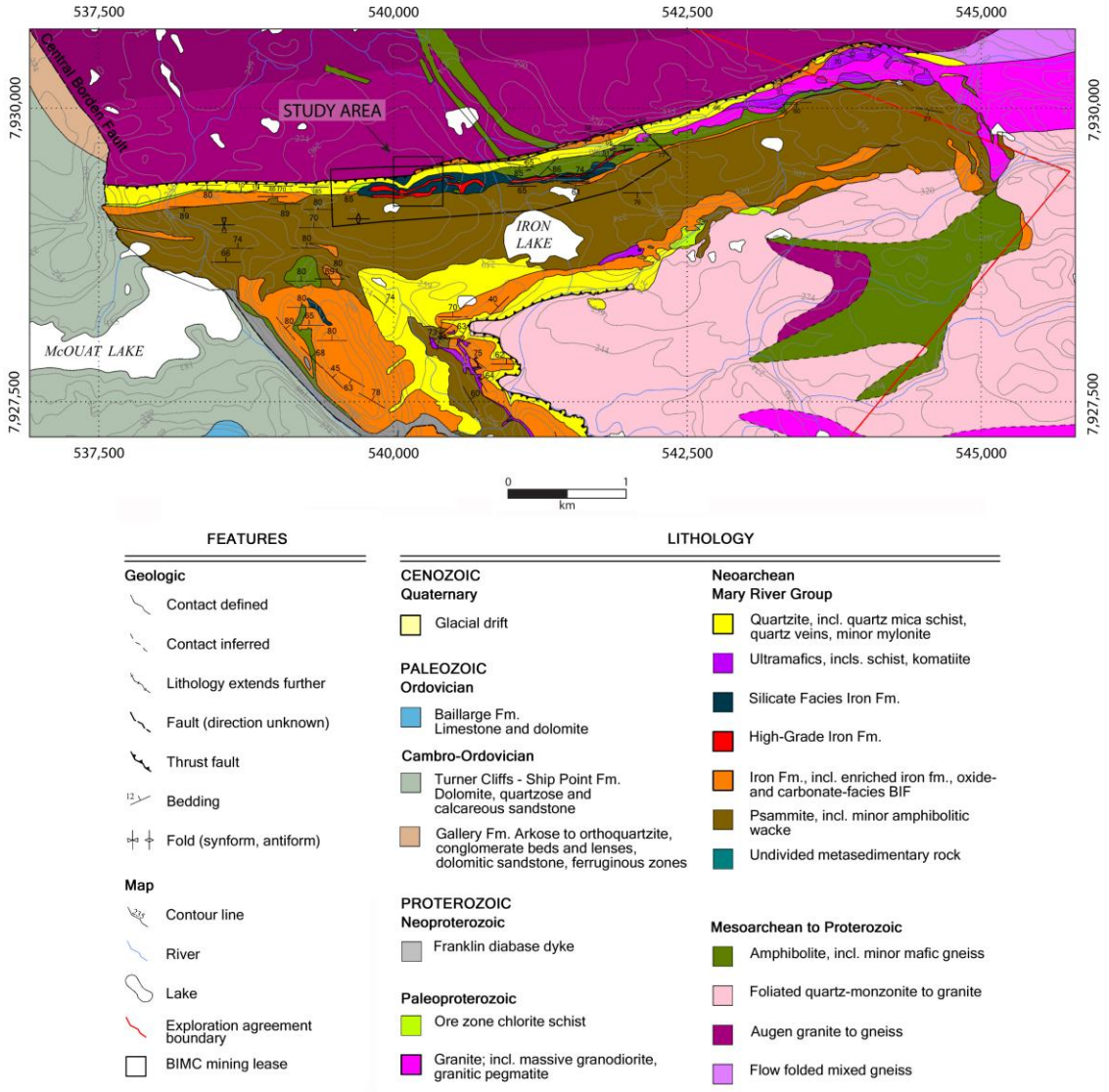

Figure 3. Geology map of study area showing north limb of the McOuat synform and location of Deposit #4 study site. The synform is bounded by detachment faults to the north and south and by the Central Borden Fault (CBF) to the west (modified from BIMC, 2014).

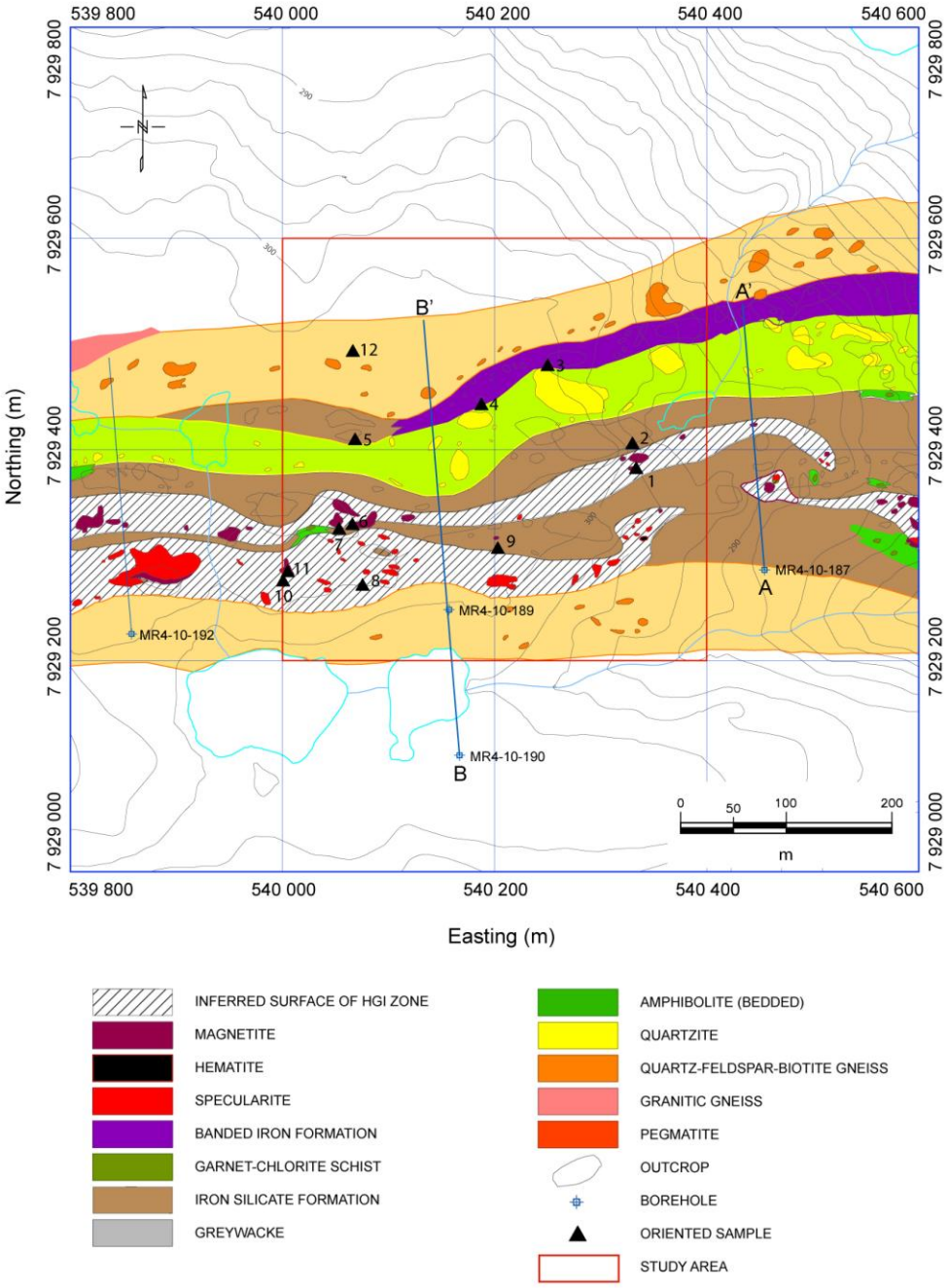

Figure 4. Deposit #4 geology map showing location of iron ore outcrops and inferred distribution of high-grade ore deposits (modified from BIMC, 2014).. High-grade ore deposits are contained within several west-east striking belts indicated by hachure. Locations of oriented paleomagnetic samples and available borehole data also shown. Cross sections A-A' (Fig. 5A) and B-B' (Fig. 5B).

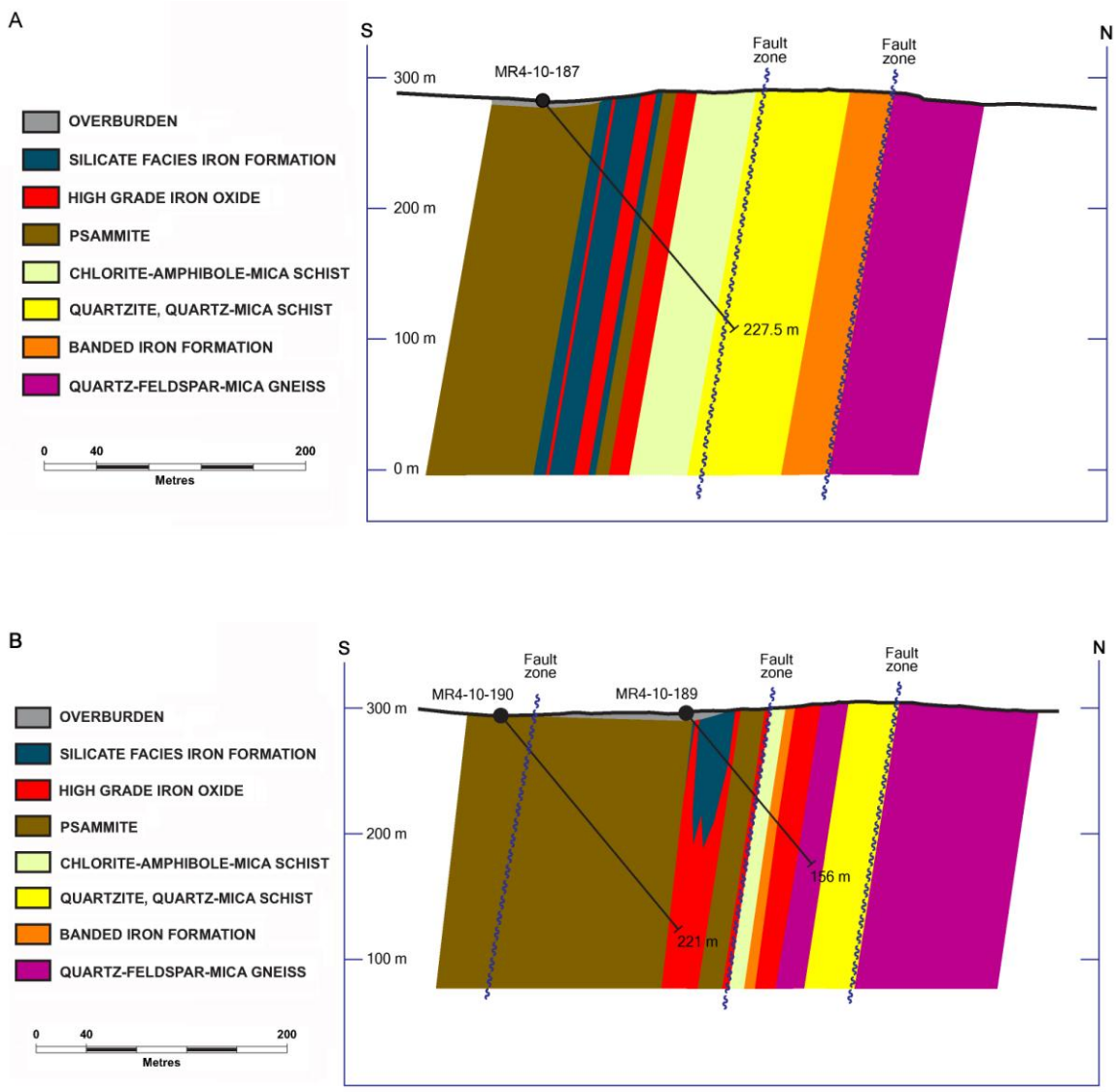

Figure 5. South-north cross-sections showing subsurface geology of Deposit #4 (modified from BIMC, 2011). Iron ore deposits are confined to several strike-parallel zones that dip southward into the McOuat synform at high angles. Locations of cross-sections are shown in Figure 4. A) Section A-A'. B) Section B-B'.

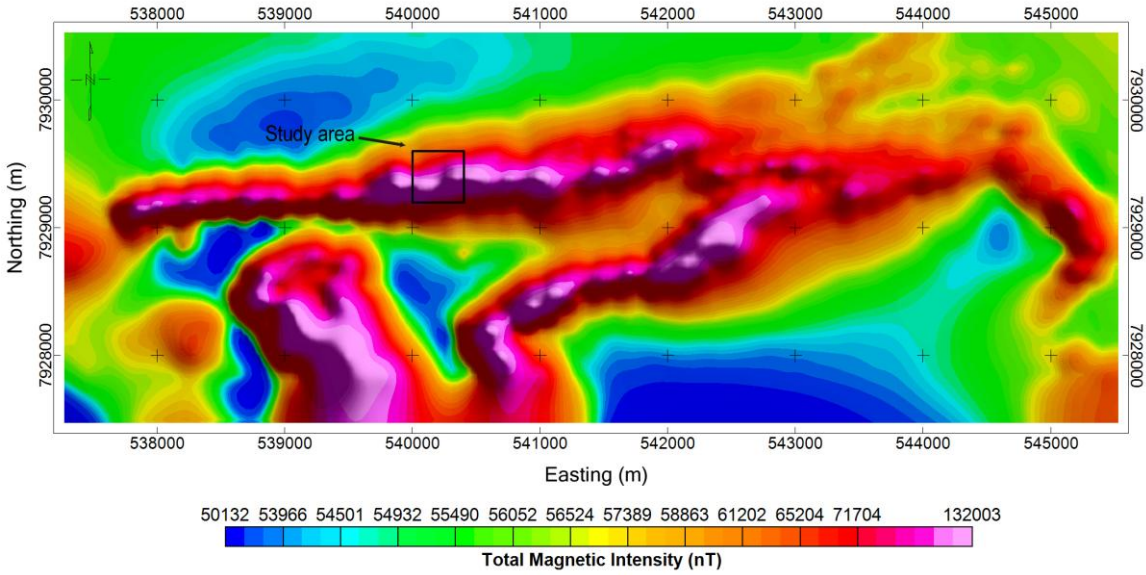

Figure 6. Total magnetic intensity (TMI) map of McOuat syncline (same area shown in Fig. 3)(data source BIMC, 2008). Heli-mag data acquired with nominal terrain clearance of 40 m and regional traverse line spacing of 200 m.

3. Methods

3.1 Vector magnetic survey

As a commercial vector magnetometer system with inertial sensors was unavailable, a custom-built magnetometer system was designed in order to meet the survey objectives. Due to the high magnetic gradient conditions and field strength at Deposit #4 (Fig. 6.) it was determined that a fluxgate magnetometer with large dynamic range would be best suited for ground-based survey work. The prototype vector magnetometer system consisted of a 3-component fluxgate magnetometer (Applied Physics model 1540; 3-Gauss per axis) mounted on a 2.7 m aluminum boom (Fig. 7A). A second Overhauser magnetometer (GEM Systems GSM-19) was pole-mounted at a height of 2 m on an aluminum frame backpack, enabling simultaneous collection of vector magnetic and TMI data over low gradient area. The fluxgate sensor orientation (pitch and roll) was recorded using a MEMS accelerometer (OceanServer OS5000) and two differential-GPS (ProMark3) receivers for azimuth measurement (Fig. 7B). The D-GPS receivers were updated at a 1 Hz rate and post-processed for a positional accuracy of < 5 cm, resulting in heading accuracy of about 1.5 degrees. Pitch and roll angles were recorded at a 13 Hz rate with an accuracy of 1 degree.

The ground-based vector magnetic survey was conducted across a 400 x 400 m (16 ha) area at Deposit #4 during a single day. A total of 21 north-south survey lines (400-m length) were acquired across the strike of the north fold limb with a nominal line spacing of 20 m (Fig. 8). West-east tie lines were collected at 50 m intervals. The fluxgate magnetometer was cycled at 50 Hz and averaged to 13 Hz in post-processing, providing a nominal inline sample interval of about 0.10 m and permitting recording of high spatial frequencies. The Overhauser magnetometer was sampled at 5 Hz to provide absolute TMI measurements for calibration of vector magnetic readings. Diurnal magnetic variations were recorded with a base station Overhauser magnetometer deployed in low gradient area at the Mary River base camp, 25 km to the southeast of the

survey site (Fig. 2). The diurnal variation in the vector magnetic components was also measured with a basestation fluxgate tri-axial magnetometer at the same location.

In order to validate the attitude correction method of the ground-based vector magnetic survey results, static vector magnetic measurements were obtained at 94 stations along Line 5 (Fig. 8) with the fluxgate sensor mounted on a 1.5 m aluminum boom fixed to a non-magnetic tripod. Prior to measurement, the sensor was carefully levelled using bubble levels and the sensor azimuth determined using dual receiver Trimble R8 survey RTK D-GPS using the method shown in Fig. 7. Vector magnetic measurements were recorded for 20 seconds at a 13 Hz sample rate to allow time averaging of the vector components. The D-GPS positions were recorded at a 1 Hz update rate and the station positions and sensor azimuth averaged over the 20 s measurement interval.

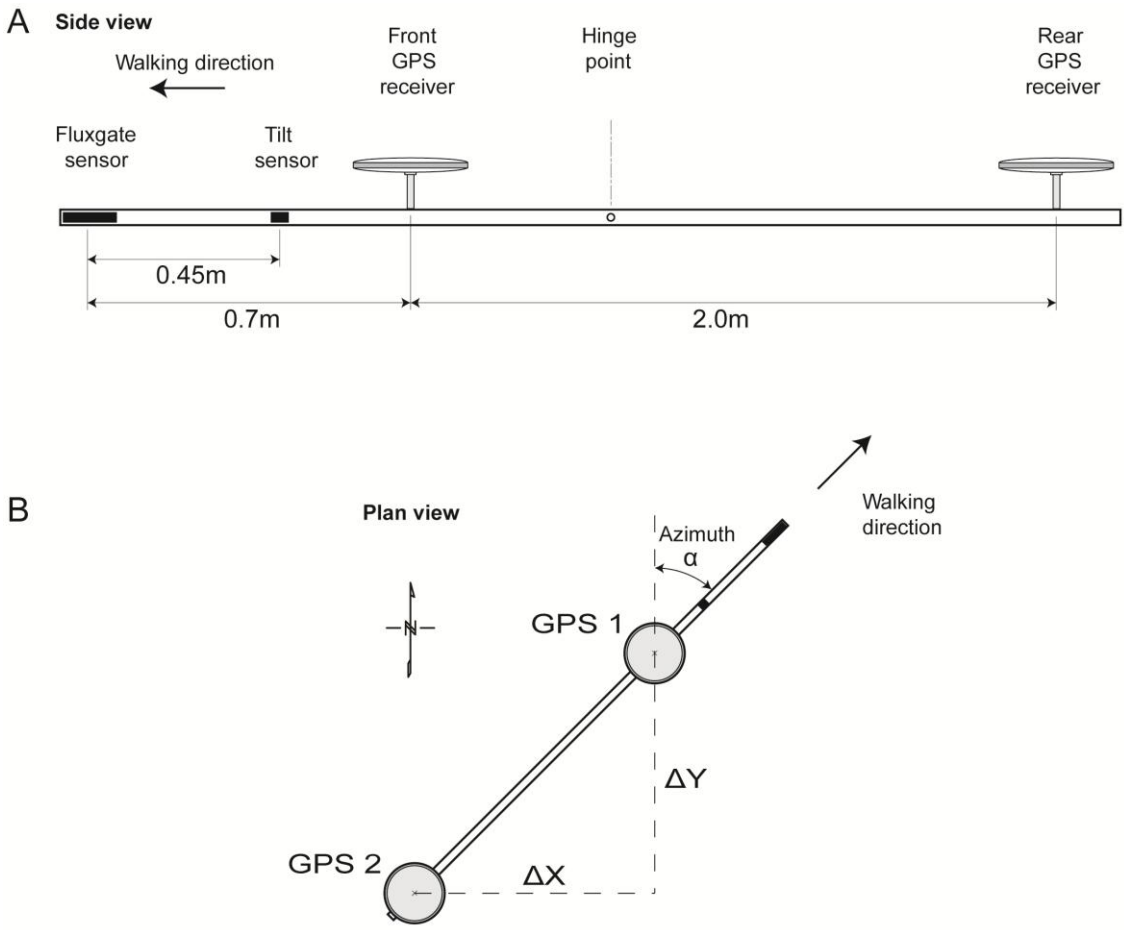

Figure 7. A) Proto-type vector magnetometer system consisting of tri-axial fluxgate sensor (Applied Physics 1540), MEMS tilt sensor (OceanServer OS5000) and two D-GPS receivers (ProMark3). An Overhauser magnetometer carried on a 2 m aluminum pole (not shown) measured the TMI simultaneously with vector magnetic measurements.
B) Sensor azimuth obtained as point-to-point vector using differential position of two D-GPS receivers.

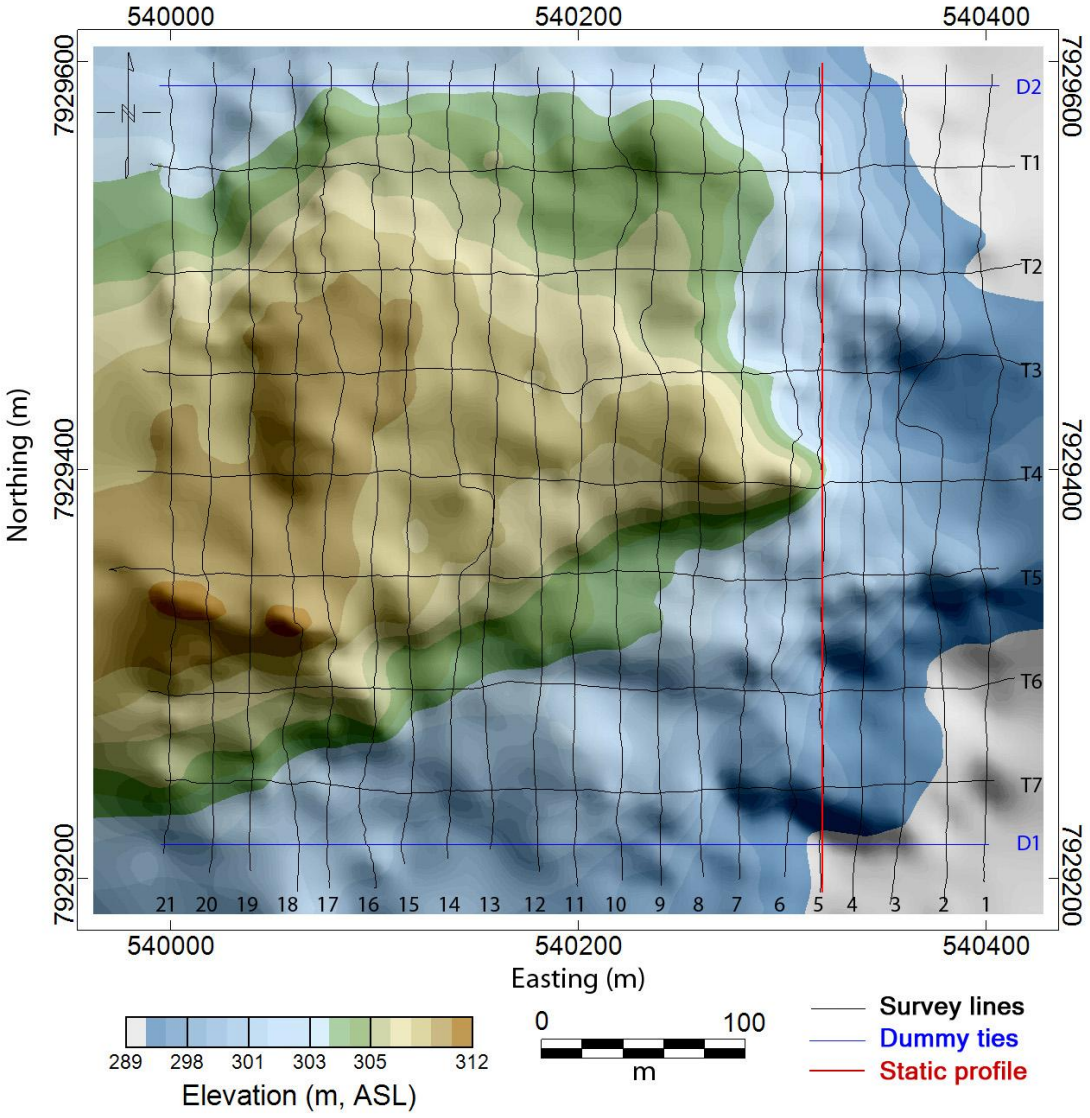

Figure 8. Digital elevation model (DEM) showing magnetometer survey grid. 21 North-South lines and 7 E-W tie lines were collected during the walking vector magnetic survey. Static vector magnetic measurements were acquired along Line 5 (marked in red) with levelled, tripod-mounted fluxgate sensor at a nominal 3 m station interval.

3.2 Data processing

The vector magnetic data processing flow is summarized here and is described in detail by Inozemtsev (2015; Chapter 2). The project data comprised four parallel data streams: Overhauser TMI data, fluxgate tri-axial magnetic components, MEMS tilt data and D-GPS positional data. All four data sets were processed in Geosoft Oasis Montaj™ software and merged in post-processing using a common time reference channel. A modified aeromagnetic processing flow (Luyendyk, 1997; Pozza et al. 2004) was used for magnetic data, and included signal de-spiking, lag and diurnal corrections. A 5-sample low-pass filter routine (LOWPASS; Fraser, 1966) was used for the MEMS sensor signal. Diurnal correction was applied based on a base-station Overhauser magnetometer. Sensor azimuth was derived from DGPS data using a trigonometric relationship (Eq. 2.6), with subsequent quadrant correction (Figure 7B).

Eq. 2.6

$$\alpha = \tan^{-1}\frac{\Delta \mathrm{x}}{\Delta y}$$

The recorded sensor pitch, roll and azimuth angles (Tait-Bryan angles) were used to correct the magnetic vector components for sensor motion and to bring all vector measurements to a common north-east-down (NED) geographic reference framework shown in Fig. 9. Attitudinal corrections employed a matrix rotation operation (Eq. 2.7) which converted attitude angles from a moving reference frame M to fixed or inertial reference frame I (LaValle, 2006):

Eq. 2.7

$$R_I^M(y,p,r) = \begin{pmatrix} cos(y)cos(p) & cos(y)sin(r)sin(p) - cos(r)sin(y) & sin(r)sin(y) + cos(r)cos(y)sin(p) \\ cos(p)sin(y) & cos(r)cos(y) + sin(r)sin(y)sin(p) & cos(r)sin(y)sin(p) - cos(y)sin(r) \\ -sin(p) & cos(p)sin(r) & cos(r)cos(p) \end{pmatrix}$$

where y,p,r represent the sensor yaw (azimuth), pitch and roll.

Following attitude corrections, the vector component maps displayed significant line-to-line corrugations, while the TMI did not. This suggested that corrugations were due to inaccuracies in sensor attitude measurements and tilt corrections. In order to minimize line levelling errors and miss-ties, each component was levelled using careful line-by-line tilt-levelling using two synthetic dummy ties located at the northern and southern ends of the survey area (Figure 8). These ties were produced by fitting a polynomial to the intersection residual errors with survey lines.

The residual magnetic vector intensity (RMVI) and residual inclination and declination were computed by vector subtraction of a constant regional magnetic vector obtained from IGRF-12 model (NRCAN, 2014)(Equations 2.3, 2.4, 2.5). The mean vector orientation measured by basestation magnetometer located at the Mary River base camp produced very similar results to the IGRF-12 model, but for technical reasons was not deployed on the day of survey. The fully-corrected total magnetic intensity (TMI) as well as RMVI and individual vector components were gridded using minimum curvature method (Briggs, 1974) with 5 m cell size and displayed using a colour-shading algorithm.

3.3 Rock magnetic properties

A total of 12 oriented block samples of representative high-grade ore types, BIF host and country rocks were collected for measurement of rock magnetic properties (Fig. 4). Block samples were sub-sampled in the lab using a 2.5 cm diamond core and a range of magnetic property measurements conducted at the McMaster University Applied Geophysics Lab. The natural remanence magnetization (NRM) was measured using a Molspin spinner magnetometer and the low-field susceptibility (κ) and anisotropy of magnetic susceptibility (AMS) were measured on a Bartington MS-2B susceptibility meter.

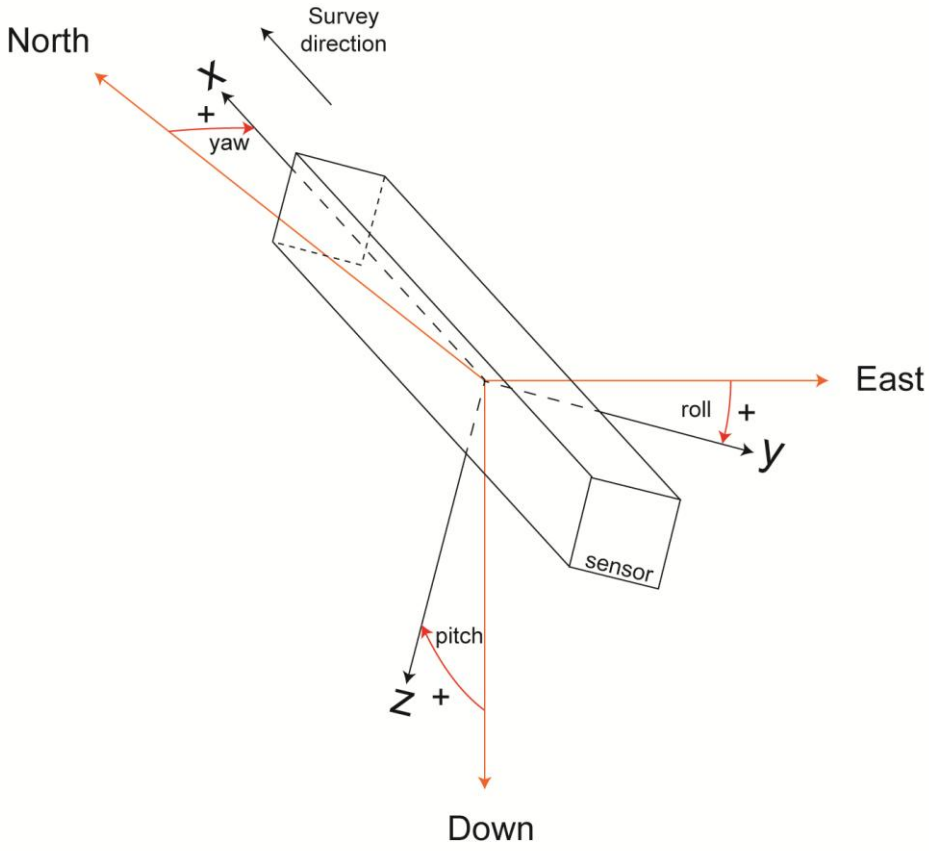

Figure 9. North-East-Down (NED) coordinate system, employed in vector magnetic survey. Sensor pitch, roll and yaw angles were transformed to NED reference framework using a matrix rotation operation.

4. Results

4.1 Total magnetic intensity (TMI) maps

The fully levelled fluxgate TMI map is shown in Figure 10. The variation in magnetic field intensity across the site exceeded 350,000 nT with an average background TMI value of about 58,000 nT. The main body of the iron ore deposit is identified by a west-east zone of high amplitude anomalies, with peak intensities of over 420,000 nT (Fig. 10). The zone of west-east anomalies is up to 125 m in width, and corresponds with a belt of high-grade magnetite, specularite and silicate iron formation outcrops on the site geology map (Fig. 4). The magnetic anomaly pattern within the ore zone shows a number of distinct maxima and minima, which correspond with the mapped location of massive magnetite ore pods with an apparent dipolar magnetic response. A northeast-southwest trending magnetic anomaly of more moderate intensity (<100,000 nT) in the northeastern quadrant of the map is associated with a narrow (< 10 m) lensate body of BIF (Figs. 4, 10). Within the high-grade ore zone a distinctive northwest-southeast trending magnetic fabric is defined by a set of magnetic lineations, which offset the strike of the west-east anomalies with an apparent left-handed displacement. These lineaments likely represent brittle faults or shear zones formed post-emplacement of the high-grade ore (see Discussion). The lineaments parallel the general trend of the Central Borden Fault to the west, and may provide evidence for deformation of MRG during the Trans-Hudson Orogen (see Discussion).

Figure 11 compares of the fluxgate and Overhauser TMI profiles acquired along Line 5 (see Fig. 10 for location). The Overhauser profile is discontinuous due to signal drop-out in high-gradient areas of the ore deposit the TMI exceeds 140,000 nT. The fluxgate TMI profile has a much higher frequency content due the greater sampling frequency (13 Hz) and records several small dipole sources that are not recorded in the Overhauser data. The fluxgate signal matches the Overhauser sensor closely in low gradient areas of the study site but over the deposit the signals diverge by up to several

hundred nanoteslas, which is due to the loss of tuning in the Overhauser as it exceeds it maximum range.

The fluxgate TMI profile shows four distinct maxima, which can be correlated with outcrops of specular hematite, magnetite and a narrow BIF unit at the north end of the profile (Fig. 11). The high-grade magnetite ore zone is characterized by TMI values that are 1.5-2 times the amplitude of hematite ores and BIF, indicating that the amplitude may be employed to discriminate magnetite from hematite ores.

Figures 12A and 12B show the analytic signal amplitude (ASA) and first vertical gradient of the TMI. The ASA is employed widely as an interpretative tool, as it produces maxima, which are centered over the magnetic source bodies regardless of the direction of magnetization (Roest et al., 1992; MacLeod et al., 1993). The ASA and vertical derivative maps highlight the presence of high susceptibility magnetite-bearing units and clearly show a northwest-southeast trending fabric within the main west-east ore zone. Both grids are show corrugations and noise produced by uncompensated levelling errors in the TMI data, which make them unsuitable for detailed magnetic interpretation.

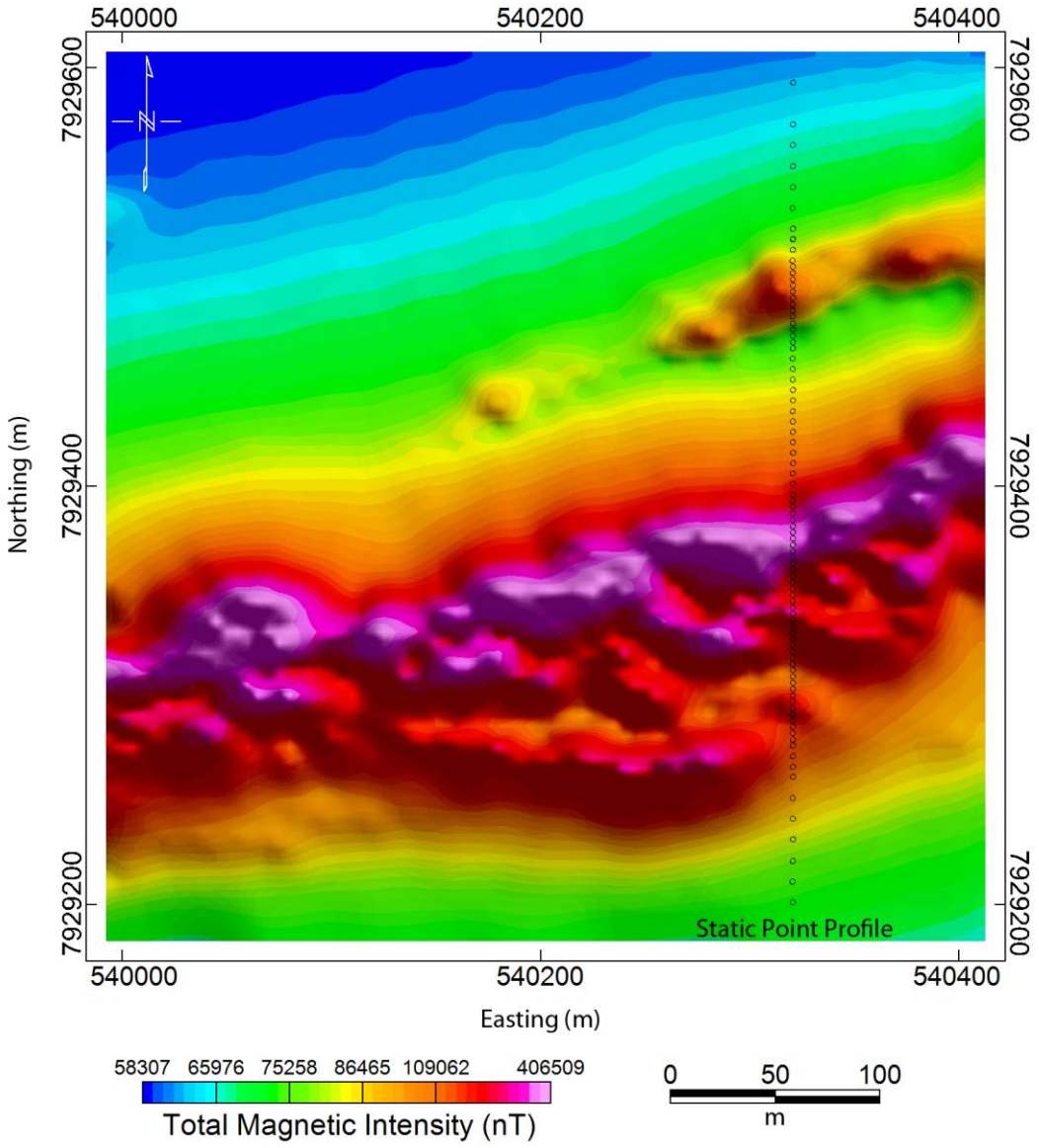

Figure 10. Fully levelled total magnetic intensity (TMI) map obtained from 3-component fluxgate data. Note maximum TMI of over 400,000 nT recorded over magnetite and hematite high-grade ore zones. Locations of static point profile stations along Line 5 are also shown.

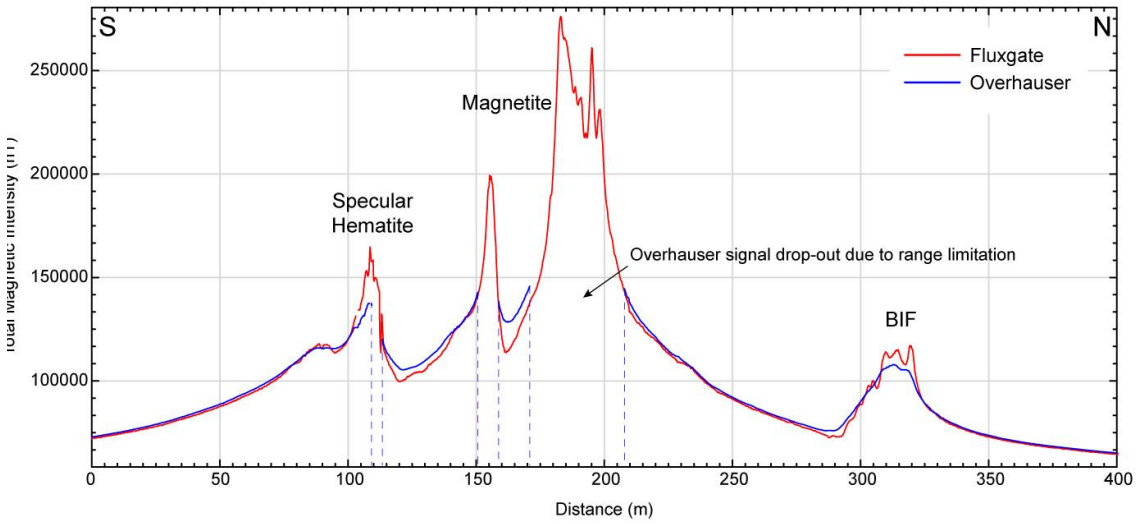

Figure 11. Comparison of TMI profiles recorded along Line 5 with Overhauser and fluxgate magnetometer system. Note gaps in Overhauser profile due to signal drop-outs produced by loss of sensor lock for intensities above 140,000 nT.

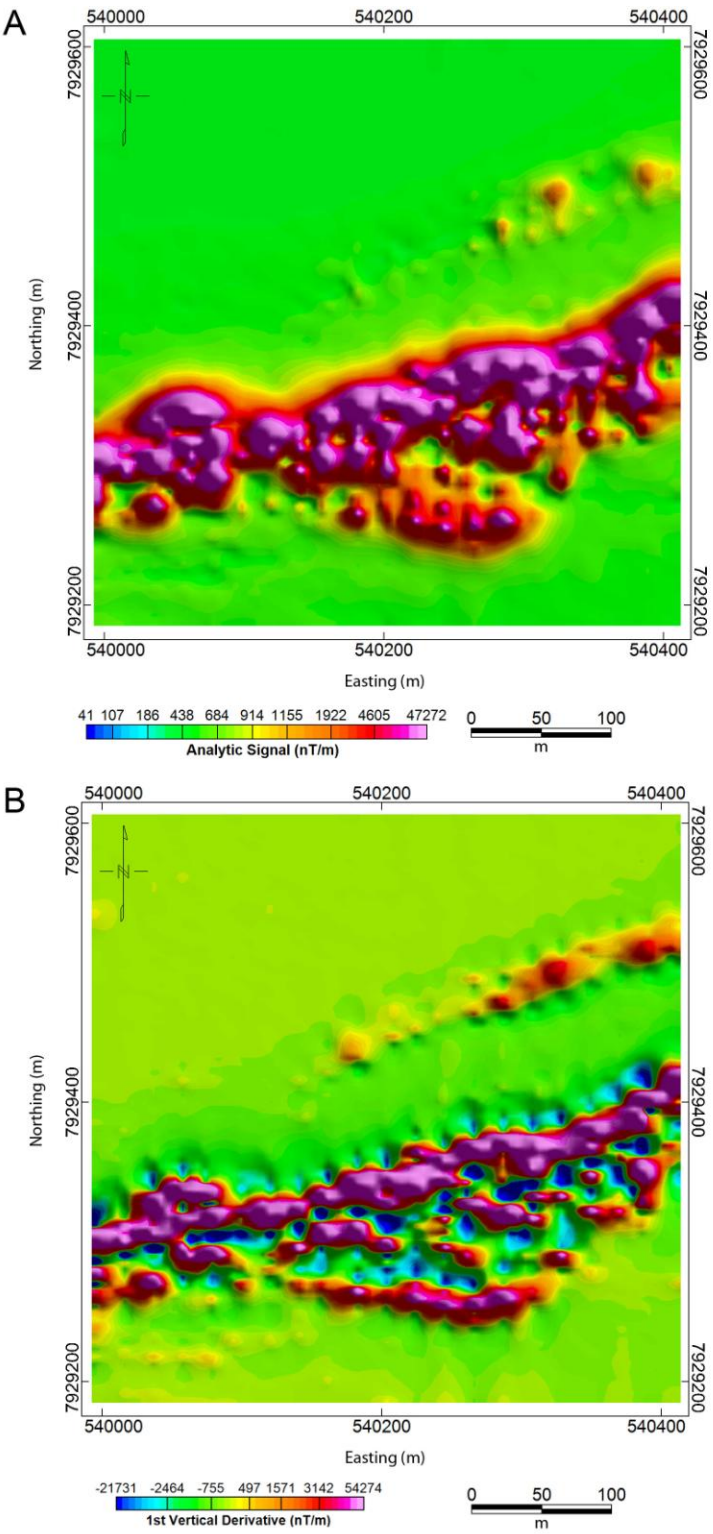

Figure 12. A) Analytic signal amplitude (ASA) calculated on levelled fluxgate TMI

4.2 Vector magnetic results

The fully-corrected magnetic vector components (x, y, z) are shown as colour-shaded grids in Figure 13 and the individual Line 5 vector component profiles in Figure 14. The static point survey measurements are also shown in Figure 14 for comparison with the walking survey data. All component maps show more evidence of line corrugation noise than the TMI due to inaccuracies in the sensor tilt corrections, but the noise levels are acceptable given the large range of the magnetic field. The static survey vector components in Line 5 closely match those recorded with the walking survey, providing verification of the attitudinal corrections applied to mobile sensor.

The x-component grid (Fig. 13A), acquired in the line direction, shows that the main west-east ore body has a distinct dipolar response with an inflection point that corresponds roughly with the amplitude maximum in the TMI map (Fig. 10). The northwest-southeast fabric visible within the ore body in the TMI map (Fig. 10) is significantly enhanced in the x-component grid, as this component is oriented N-S across the strike of the deposits. The x-component profiles in Figure 14 also show that individual anomalies associated with outcrops of specularite and magnetite ores are distinct dipolar anomalies. The peak-to-peak variation of the main west-east trending anomaly reaches 320,000 nT, while the anomaly over the BIF unit in the northeast quadrant of the map area is about 38,000 nT.

The y-component grid (Fig. 13B) also identifies high-grade ore anomalies as dipoles, however the peak-to-peak variation is less pronounced (< 180,000 nT) and the noise levels are generally greater due to the lower range of magnetic intensity in the west-east component. The magnetic fabric shows less coherence, consisting of multiple dipolar targets but without a well-developed NW-SE linear fabric.

The z-component (Fig. 13C) map displays a similar overall anomaly pattern to the TMI grid, but with enhancement of the magnetic lineaments defining the NW-SE magnetic fabric in the main ore zone. The lineaments clearly cross-cut the west-east line of dipoles defining the magnetite west-east ‘ridge’ and are sub-parallel with the nearby

Central Borden Fault, which is oriented northwest-southeast with a strike of approximately 320-140º (Fig. 3). The lineaments offset the magnetite ridge with a sinistral displacement of about 20-30 m and are interpreted as fault or shear zones with a possible structural affinity with the CBF. The z-component magnetic intensity variation is large (>340,000 nT) compared with the other two components, indicating that the primary magnetization direction in the ore deposits is directed downward and approximately parallel with the bedding plane.

In order to better understand the spatial variations in the magnetic vector orientation, the RMV inclination and declination were plotted in map view (Fig. 15). In this image, the inclination is shown as a colour-shaded image and the declination with arrows. The declination arrows show that the field vector across the site systematically points towards the high-grade magnetite and hematite ore zone, even in the northwest quadrant of the map, which is more than 200 m away from the main iron ore source body. Within the magnetite-rich portion of the ore body, the declination is deflected locally towards high strength anomalies, which likely represents local pods of magnetite (Fig. 15). The declination differs significantly from the background geomagnetic field, which is declined at about 37 degrees west. The inclination grid, because it is very sensitive to local magnetic sources, clearly shows the northwest-southeast magnetic fabrics visible in the horizontal component grids (Fig. 13).

Profiles comparing the total magnetic vector (TMV) and residual magnetic vector (RMV) inclination and declination for Line 5 are shown in Fig. 16. The RMV profile shows enhanced frequency content as compared to the TMV profile. The close correlation between the static point measurements and walking survey measurements is again visible. This correlation is also shown in the form of cross-plots on Fig. 18.

Figure 17 illustrates the changes in the magnetic vector orientation along the Line 5 profile, representing a characteristic cross-section of the deposit. Also shown are the TMI profile, and the regional background field orientation (NRCAN, 2014). The three main peaks in total field coincide with specular hematite, magnetite and BIF-dominated zones mapped on the geology map. These peaks align with the major changes in vector

orientation, both inclination and declination. The arrow plot of the inclination is especially interesting, revealing the dramatic change in vector direction across the site profile.

Histograms showing the frequency distributions for the RMVI measured at mapped ore outcrop locations are shown on Fig. 19. The locations of ore outcrops used in this analysis are shown in Fig. 4. The same RMVI scale is used for the histograms in Figure 19A-C. The histograms show that ore types are associated with a distinct range of RMVI values. The BIF has the narrowest range of (39,034-68,068 nT) with a mean value of 52027 nT. The specular hematite RMVI distribution is much broader (51,714-232,672 nT) and strongly skewed towards the lower end of the scale, with a mean of 90,357 nT. The magnetite distribution has a dramatically wider range of 67,000-362,700 nT, and shows a distinctly bi-modal distribution with modes at about 50,000 and 150,000 nT. The lower mode is close to the value for specularite and may indicate the presence of hematite pods or interbeds with the main mass of high-grade magnetite iron ore. The overall study site distribution is shown in Fig.19D, and is strongly skewed towards the lower end of the scale, dominated by the lower intensities of weakly magnetic schists and low magnetic susceptibility psammite host rocks.

A histogram analysis of the RMV inclination was performed using the same outcrop locations (Fig. 20). Here the BIF (Fig. 20A) again shows a strong skew towards lower inclination values with a mean of 25º. Both magnetite (Fig. 20B) and specular hematite (Fig. 20C) show much wider ranges of inclination, with magnetite distribution containing two dominant modes of 30º and 70º. The overall RMV inclination distribution across the entire site (Fig. 20D) is skewed towards lower values, with a mean of 25º.

Figure 21 uses equal area projection stereonet plots to illustrate statistical summary of the RMV orientation. All outcrops are summarized in part A, with the mean vectors identified with circles. The diameter of the circle is proportional to the overall spread of the distribution. The ore types are shown in B,C and D with the corresponding 1% vector density contours. BIF shows the most consistent distribution, with the mean vector pointing south at 173º-188º. The magnetite ores show the largest spread, with a

mean vector oriented 182º-159º. Specular hematite has a slightly smaller spread with a mean vector pointing 344º-355º.

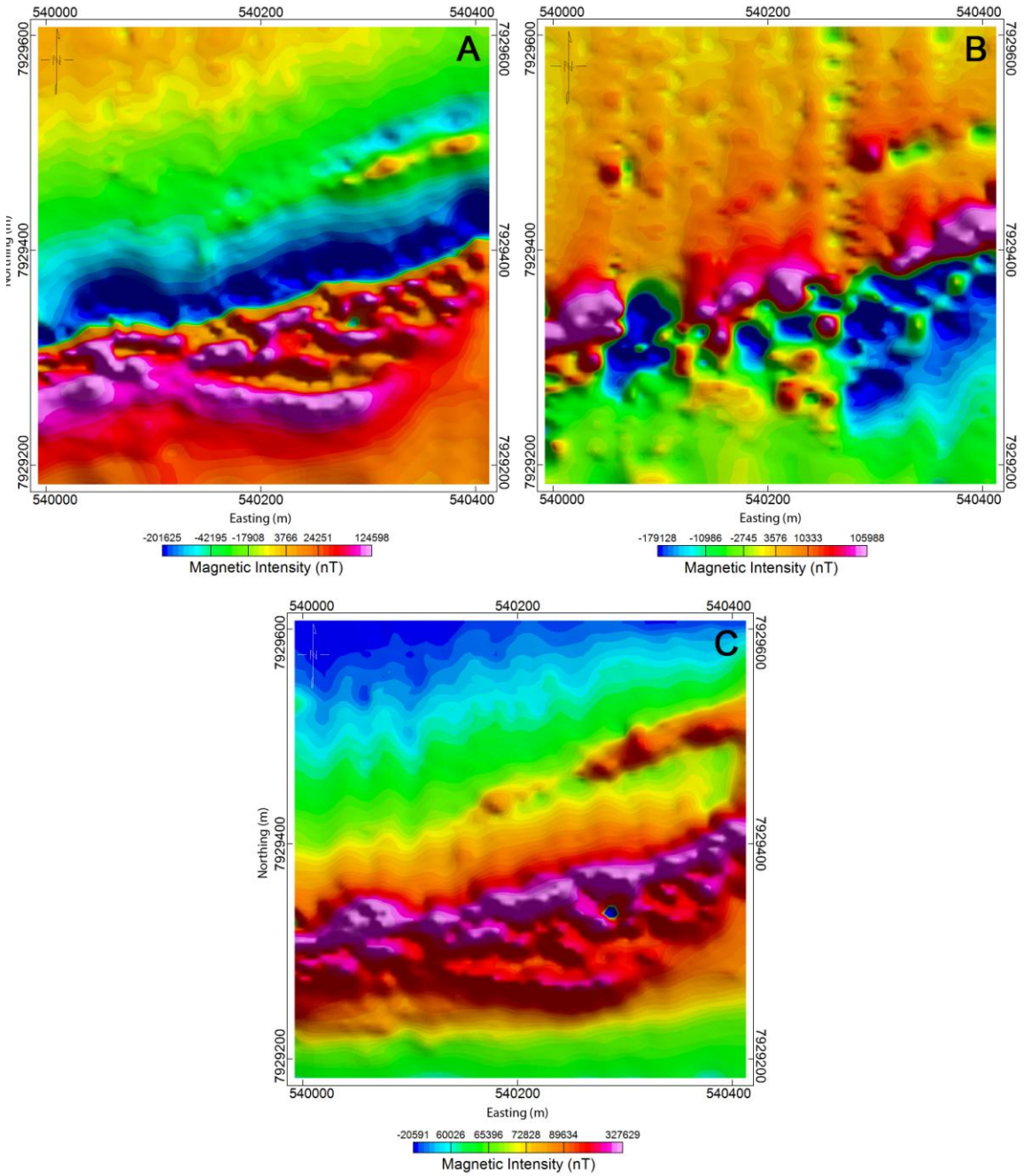

Figure 13. Vector component maps. A) X-component (positive: North). B) Y-component (positive: East). C) Z-component (positive: Down).

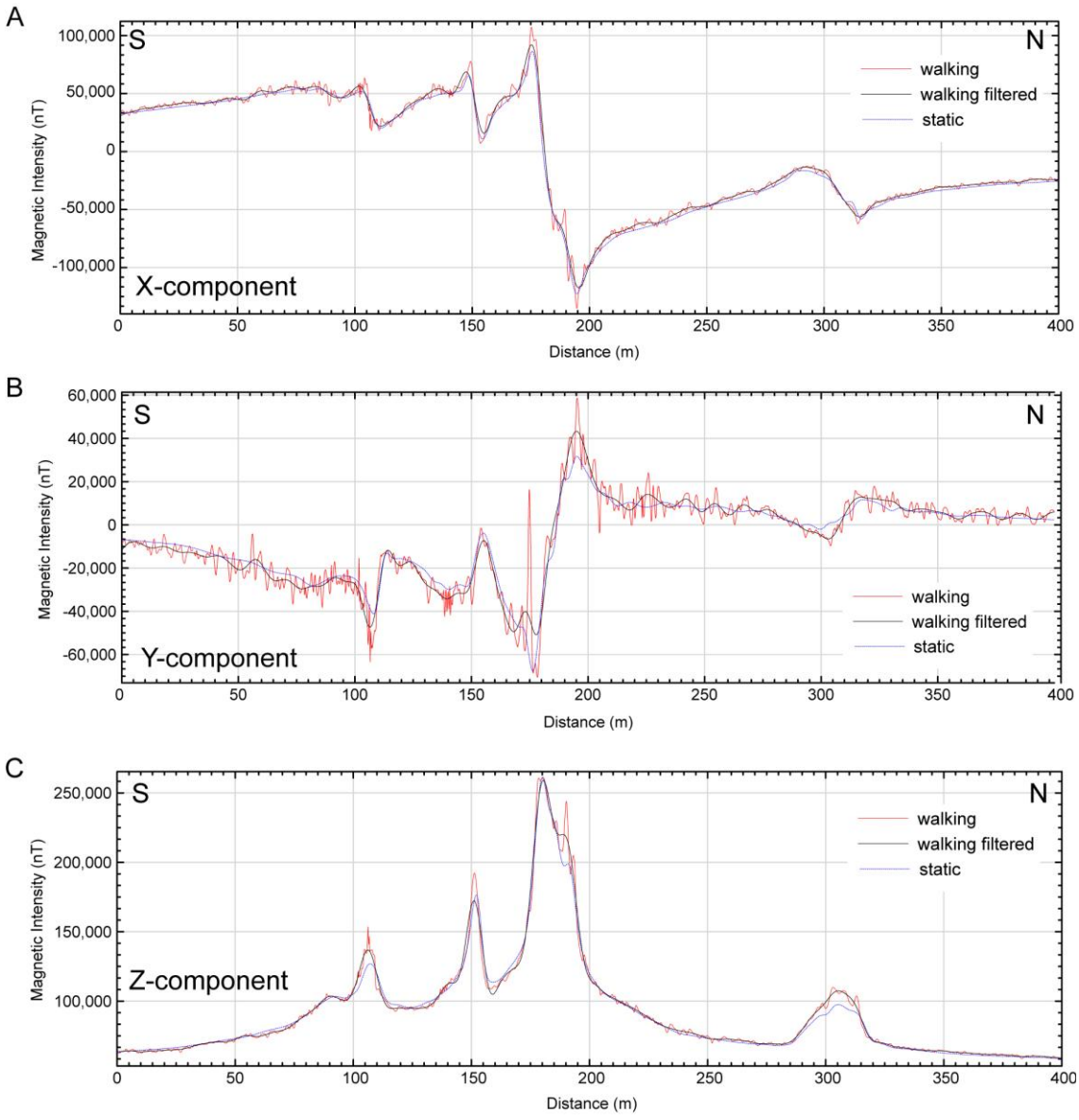

Figure 14. Comparison of walking and static vector measurements for Line 5. Note anomaly peak in Z-component correpsonds with inflex in X and Y.
A) X-component (North). B) Y-component (East). C) Z-component (Down).

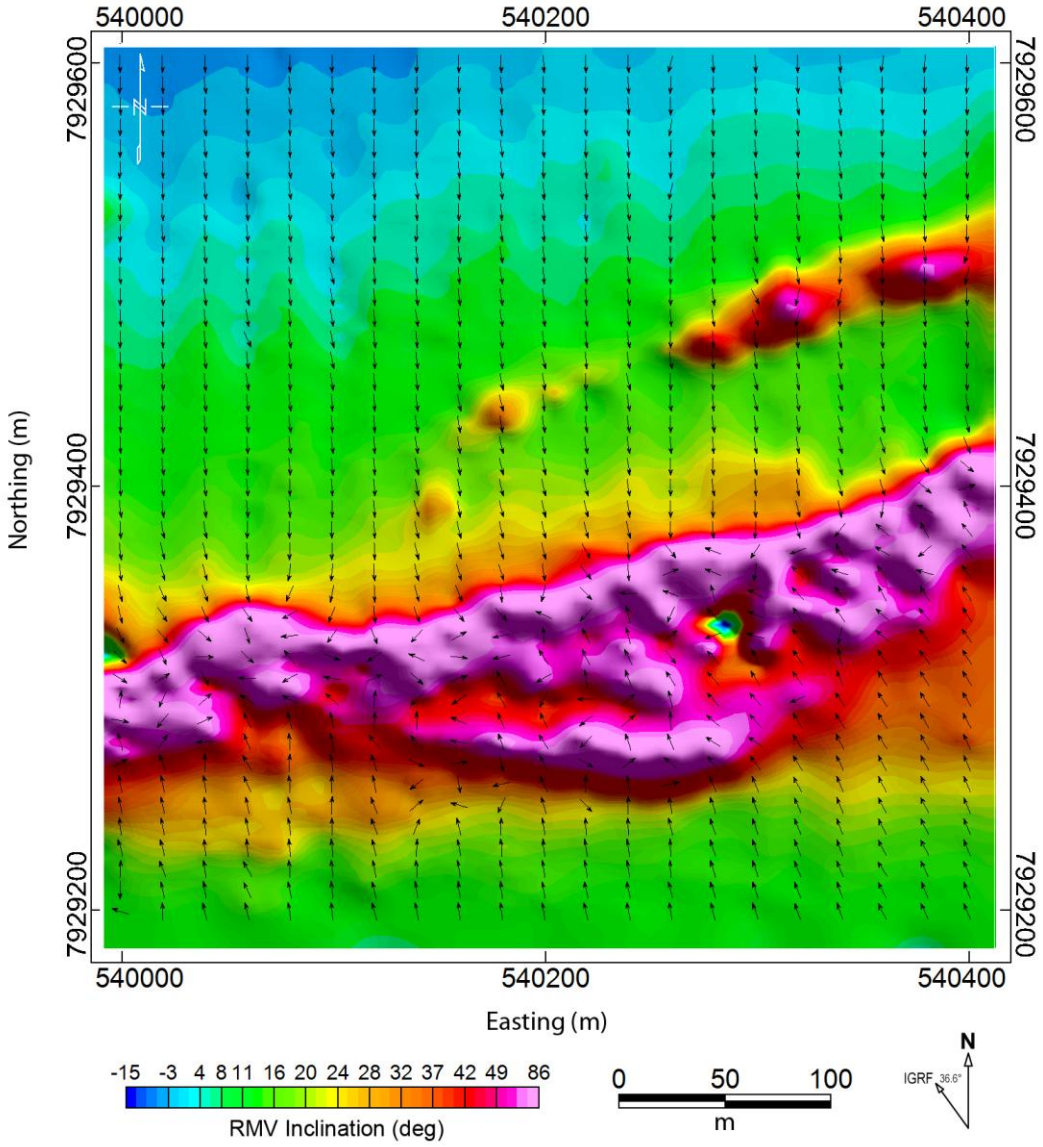

Figure 15. Orientation of the residual magnetic field vector (RMV). Vector inclination shown as colour-shaded image and declination indicated by arrows (regional geomagnetic field (IGRF) employed in vector subtraction: declination 36.6°W, and inclination of 85.4°).

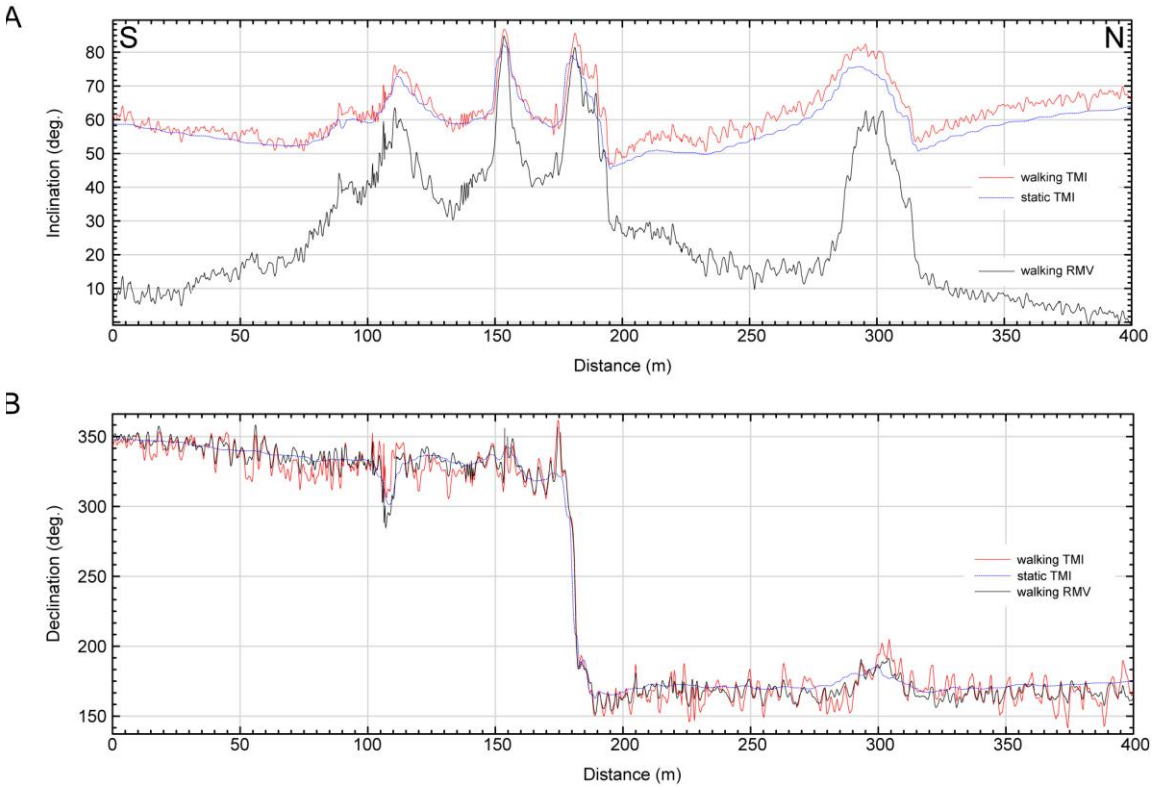

Figure 16. Profile comparison of vector inclination and declination of total magnetic vector (TMV) versus residual magnetic vector (RMV) acquired on Line 5 with walking survey and static fluxgate measurements. A) Inclination. B) Declination. Note enhanced resolution of anomaly patterns in RMV inclination following subtraction of regional vector.

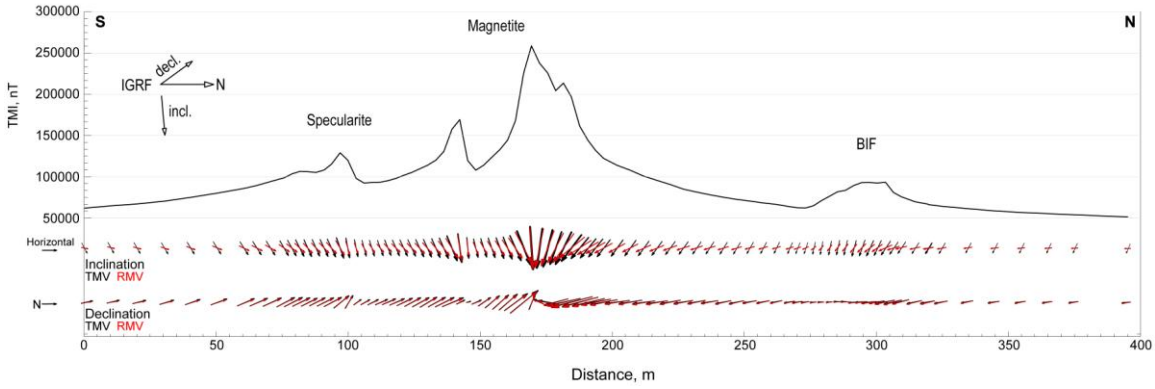

Figure 17. Profile comparing inclination and declination of total magnetic vector (TMV) (black arrows) with those of residual magnetic vector (RMV) (red arrows) for Line 5. Data collected during static fluxgate measurements. Also shown are the dominant ore types associated with TMI peaks, and the regional background field (IGRF) inclination and declination.

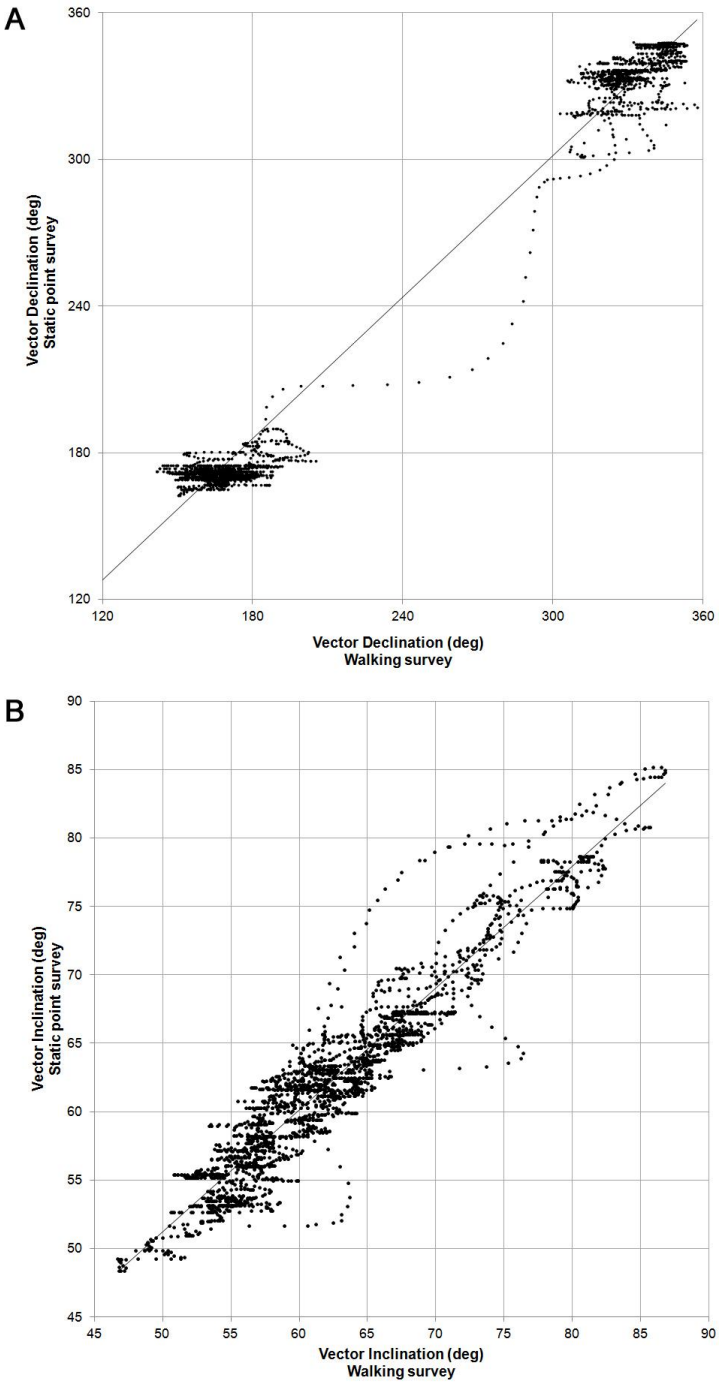

Figure 18. Cross-plots of vector orientations comparing walking and static measurements acquired along Line 5. A) Vector declination (R^2 = 0.967). B) Vector inclination (R^2 =0.899)

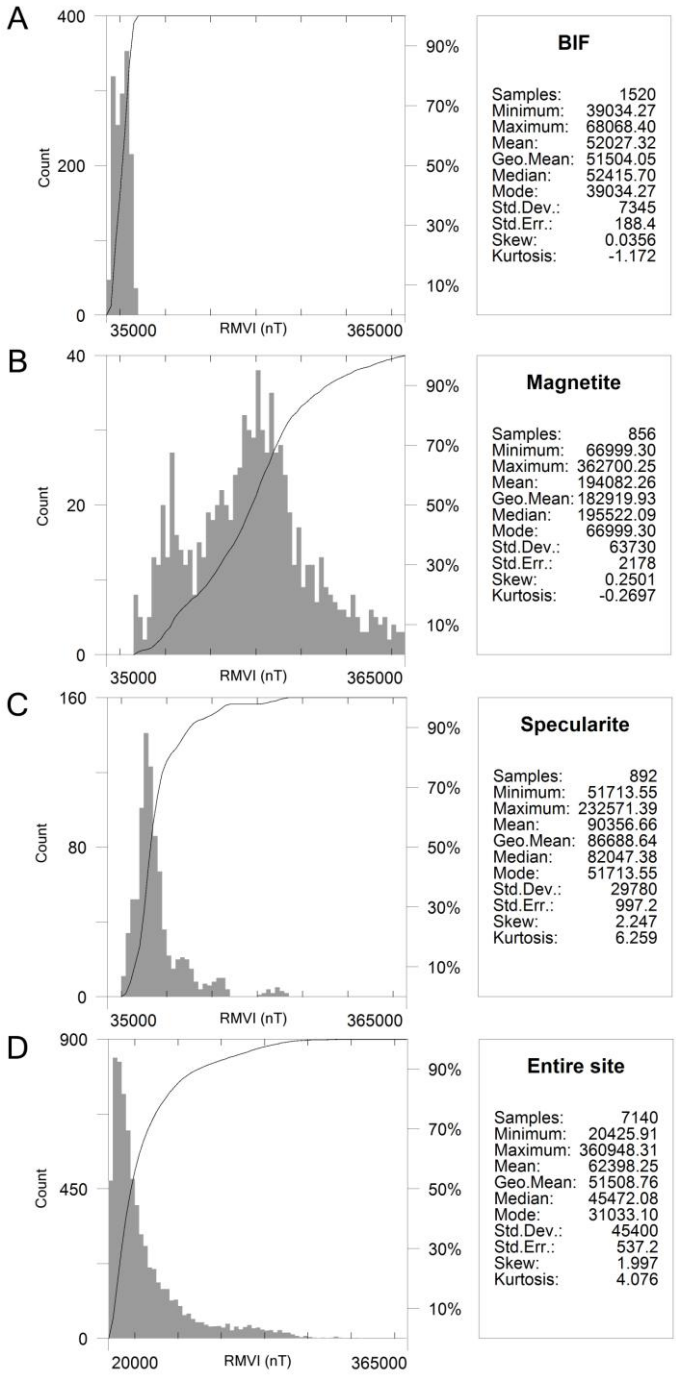

Figure 19. Frequency distributions of residual magnetic vector intensity (RMVI) measured at mapped outcrops at Deposit #4 (see Fig. 5). A. BIF (15 outcrops, 1520m^2 total). B. Specularite-hematite ore (23 outcrops, 892 m^2) and C. Magnetite ore (11 outcrops, 856 m^2 total). D. Frequency distribution of RMVI for entire survey area. Note distinctive ranges of magnetic intensity (amplitude) and sample means for BIF and high-grade ores. Magnetite ore bodies (C) have a distinctly bi-modal distribution, with a minor peak 50,000 nT, likely reflecting presence of specularite-hematite within areas mapped as high-grade magnetite.

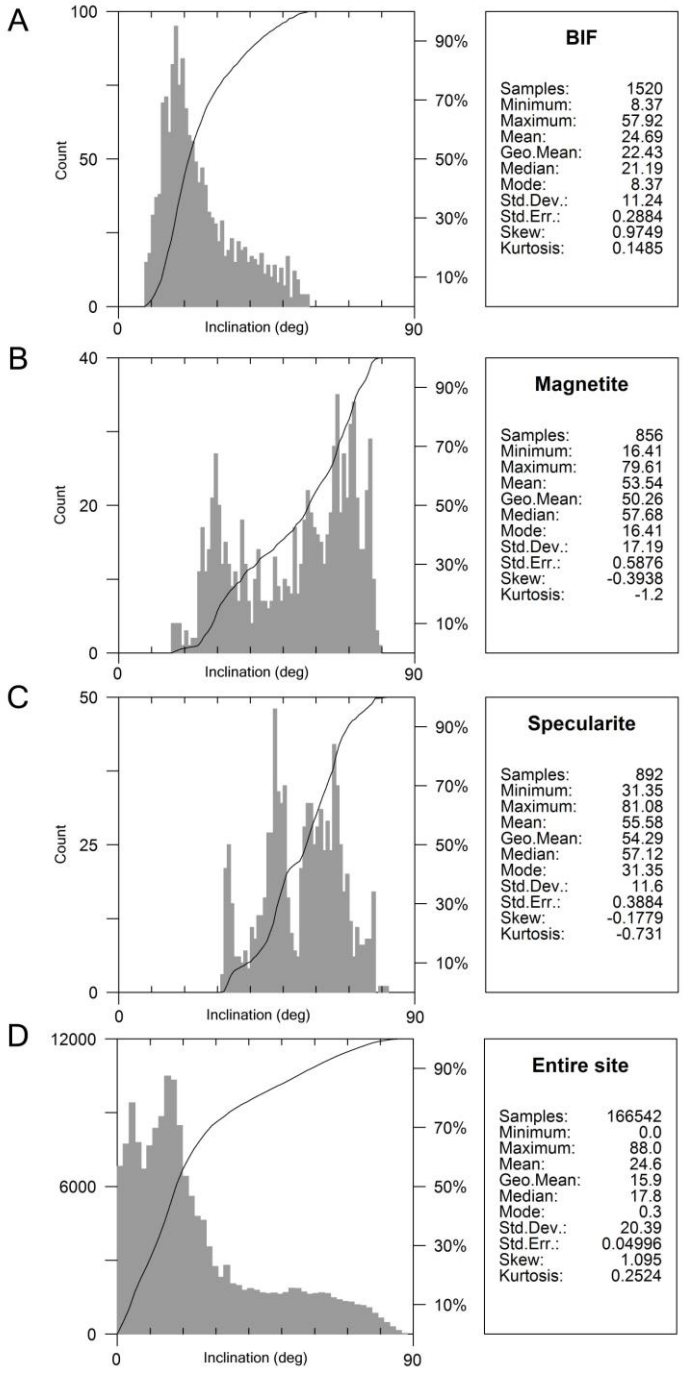

Figure 20. Frequency distributions of residual vector inclination (I_{RES}) measured at mapped outcrops at Deposit #4 (see Fig. 4). A. BIF (15 outcrops, 1520m^2 total). B. Magnetite. C. Specularite. D. All outcrops.

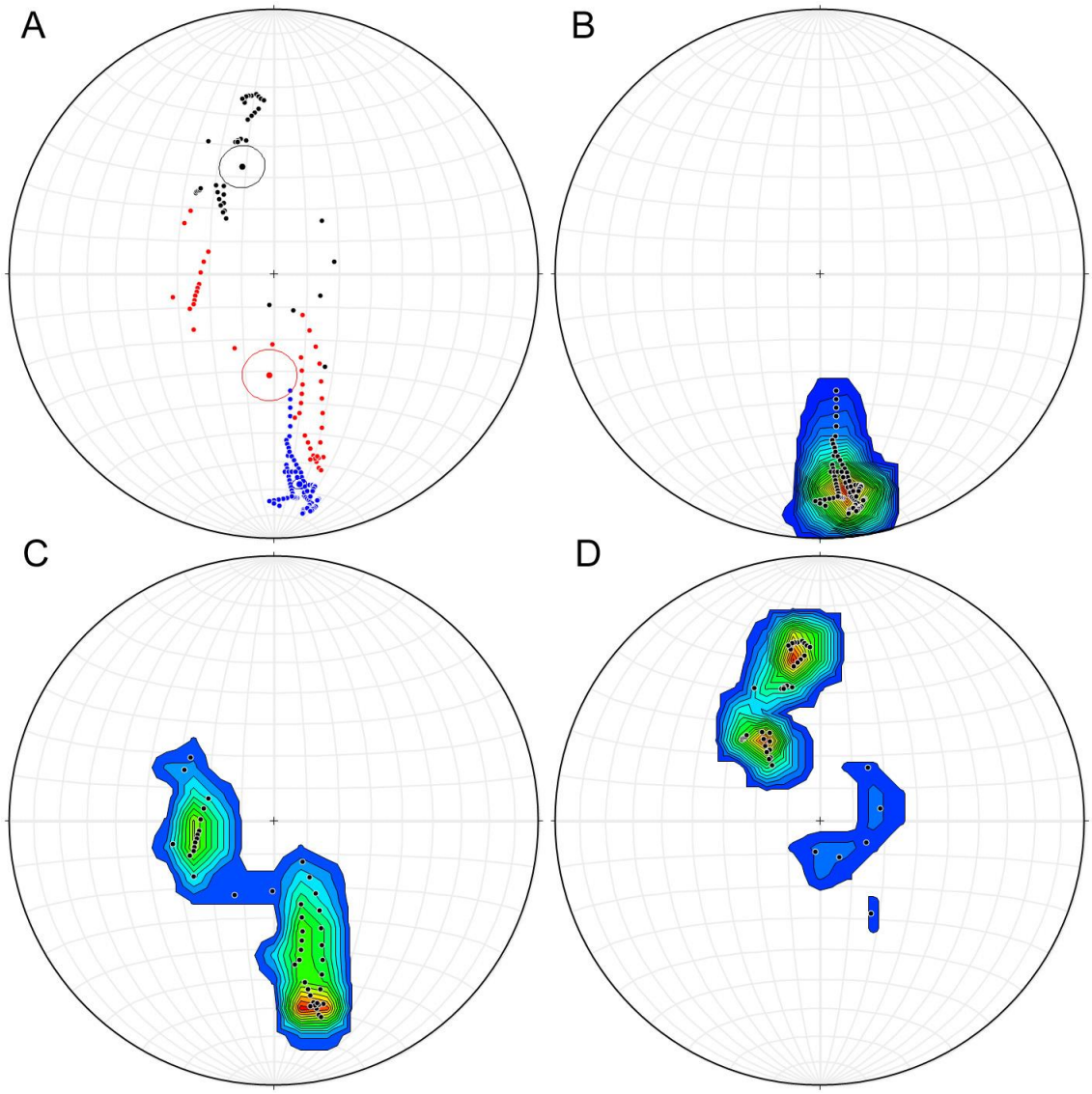

Figure 21. Stereonet plots showing residual magnetic vector orientation determined from outcrop areas of high-grade ores and BIF host rocks. A) All outcrops plotted with vector mean indicated by circles (blue = BIF, red = magnetite, black = specular hematite). B) BIF vector density contours. C) High-grade magnetite contours. D) High-grade specular hematite contours.

4.3 Rock magnetic properties

The results of rock property measurements are summarized in Table 1. The iron ore and BIF classification system is based on the total iron content and dominant mineral phase, following the scheme developed by BIMC (2008). The scheme classifies high-grade iron formations (HIF) as having > 50% total iron, and includes HIF magnetite (> 50% Fe as magnetite) and HIF specularite (> 25% Fe as specular hematite). Banded iron formations are classified as un-enriched BIF (< 25% Fe) and enriched BIF (EBIF > 50% Fe). A classification of EBIF magnetite is assigned when > 60% of iron content is attributed to magnetite.

HIF magnetite ores are characterized by high values of NRM (0.3-8.6 Am^{-1}) and high magnetic susceptibility (> 2.5 SI). HIF magnetite ores show low anisotropy (AMS 1.08-1.1) compared to BIF ores (AMS 1.29-1.83). The Q values for HIF magnetite range between 0.2-0.7 for fine-grained ores and up to 5.2 for coarse HIF magnetite. The high Q-value for coarse-grained HIF magnetite found at Deposit #4 indicates the presence of significant remanent magnetization. Depending on the dominant iron oxide, BIF ores are characterized with low Q values for hematite and magnetite (0.1-0.2) to very high values (30.2-107.3) for specular hematite. The specularite and hematite ores have a lower range of susceptibility (3.9×10^{-3} – 1.02 SI) and NRM values (0.02 – 0.54 Am^{-1}) than magnetite ores, with susceptibilities of 2.5-2.87 SI and NRM ranging between 0.29 – 8.61 Am^{-1}.

The large remanence and Q values for magnetite would require special considerations to be made in any attempt to model the underlying geology. Clark (2014) shows that in high-susceptibility sources the direction of induced magnetization can differ significantly from that of the inducing field, even if the remanence is negligible and susceptibility is isotropic. This is caused by a self-demagnetizing effect acting in non-equidimensional sources, and deflecting the induced magnetization towards the plane of sheet-like sources. They state that corrections for self-demagnetization are required for materials with susceptibility 0.1 SI and greater. Seven of the twelve samples listed in Table 1 require such a correction, and for six of them this correction would be crucial.

The remanence vector orientations are plotted for all samples on an equal area stereonet in Figure 22, and colour-coded by sample lithology. The remanence vector directions varied within each sample, with some samples showing better clustering and consistency. Samples that show good clustering include BIF specularite (#3), High Grade Iron Formation (HIF) Specularite (#8) and Chlorite amphibole schist (#2). The remanence vector could not be determined for sample #10 that became fragmented during lab tests.

Table 1: Summary of the rock magnetic property measurements for 12 oriented iron ore and host rock samples. Note high NRM magnetite ore samples (9, 10) and large Q values for specularite samples (3, 8). The remanence vector direction is the *in situ* NRM vector, without correction for folding.

Sample	Rock Type	Density	Susceptibility	Anisotropy	Anisotropy	NRM	Q ratio	Avg. Remanence vector	
		gcm^{-3}	SI	%	Max/Min	Am^{-1}		Decl.	Incl.
1	HIF Magnetite	4.75	2.6243	9	1.10	0.2981	0.2	124	46
2	Chlorite Amphibole Schist	2.89	0.0104	28	1.32	0.0086	1.4	172	32
3	BIF Specularite	3.43	0.0097	56	1.83	0.1020	30.2	90	45
4	BIF Hematite	2.94	0.2057	38	1.49	0.0178	0.1	190	54
5	Chlorite Amphibole Schist	2.91	0.0163	76	2.17	0.0072	0.8	162	54
6	EBIF Magnetite	4.60	2.5299	9	1.09	0.3475	0.2	198	25
7	EBIF Magnetite	4.64	2.6208	25	1.29	0.3680	0.2	24	32
8	HIF Specularite	5.21	0.0039	22	1.25	0.2151	107.3	232	25
9	HIF Magnetite (coarse)	5.06	2.8707	11	1.08	8.6120	5.2	101	15
10	HIF Magnetite	4.89	2.5334	8	1.08	1.0698	0.7	-	-
11	Hematite	5.06	1.0219	46	1.59	0.5430	0.8	316	5
12	Quartz augen biotite schist	2.69	0.0001	21	1.23	0.0000	0.2	220	-8

Abbreviations: **HIF**: High-grade iron formation (>50% total iron content); **HIF Magnetite**: >50% total iron, of which >60% is in magnetite. **BIF**: <25% total iron content. **EBIF**: Enriched Banded Iron Formation (close to 50% total iron). **EBIF Magnetite**: Enriched BIF with 50% total iron, of which > 60% is in magnetite. **HG Specularite**: >25% of total iron is in specularite. (BIM, 2008).

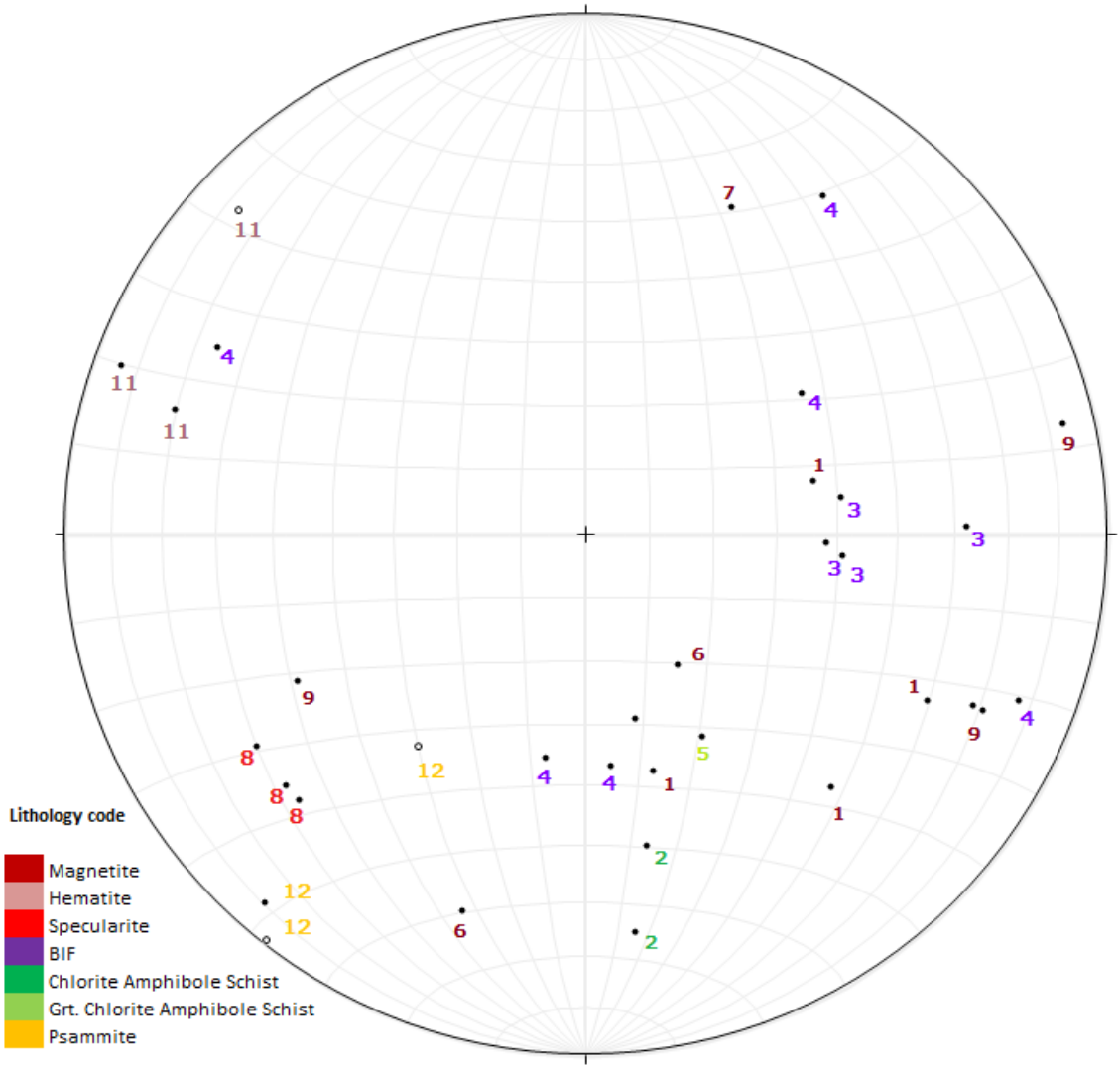

Figure 22. Equal area stereoplot showing the distribution of the measured remanence directions in the oriented samples. Sample numbers are colour-coded by sample lithology. Sample #10 is missing due to being fragmented during lab tests.

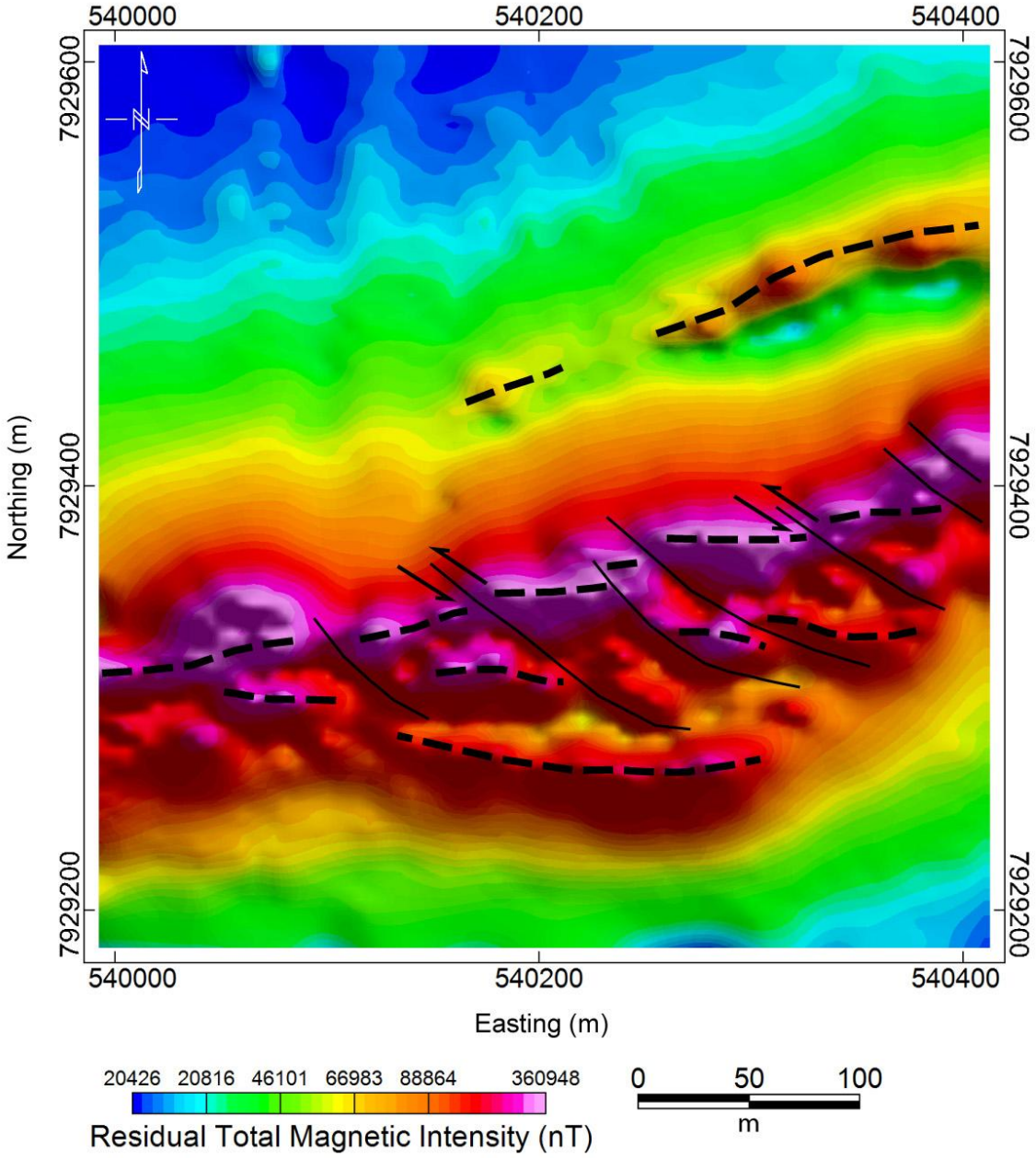

Figure 23. Residual magnetic vector intensity (RMVI) map with interpreted magnetic lineament patterns. North-East – South-West trending lineaments are interpreted as sinistral faults/shears offsetting the strike of the ore body with an apparent horizontal displacement of about 10 m.

5. Discussion

5.1 Ore deposit structure

The results of this study demonstrate that vector magnetic methods can provide important baseline information for interpretation of ore deposit geological structure. The enhanced measurement range of the fluxgate magnetometer enabled mapping of magnetic intensities of >400,000 nT across the main body of the high-grade iron ore deposits (Fig. 10). The fluxgate TMI and RMVI maps yield a dramatic improvement in resolution of anomaly maxima and delineate complex dipolar magnetic sources, which were not imaged in previous scalar magnetometer surveys (e.g. Fig. 6). Figure 24 shows the site geology map overlaid on the RMVI. The west-east belt of high-grade magnetite ore corresponds closely with the zone of highest magnetic intensity. The pattern of complex dipolar anomalies within this zone indicates that the high-grade deposits are not simple tabular bodies, but are instead characterized by podiform magnetite deposits, with a general west-east strike (Fig. 23).

The northwest-southeast trending fabric defined by magnetic lineaments within the high-grade ore zone indicates the presence of faulting or shearing of the MRG and suggests a complex and likely multi-stage deformation history. Four major phases of tectonic deformation have been recognized at Mary River (Johns and Young, 2006) but the dominant regional metamorphic overprint is related to the 1.9-1.8 Ga Baffin Orogen (Jackson and Morgan, 1978; Jackson 2000). The Baffin Orogen began with a phase of contractional deformation and northwest-directed thrusting at ca. 1850-1845 Ma, followed by significant anatexis and tectonic thickening of crust (Bethune and Scammell, 2003). This was followed by a late phase of brittle deformation, normal faulting and crustal exhumation associated with the extension of the Baffin Orogen (ca. 1800 Ma). The northwest-southeast trending Central Borden Fault (CBF), located 2 km to west of the study site (Fig. 3), was developed during this extensional phase. The northwest striking lineaments, indicating fault offsets within the ore body (Fig. 23), parallel with the

strike of the CBF and likely represent brittle faults or shears formed within the damage zone of the CBF. The northwest-trending magnetic fabric is dominated by linear magnetic lows (Fig. 23), possibly recording the movement of hydrothermal fluids along fracture zones and the change of magnetite to martite ores, causing a local reduction in rock magnetic susceptibility.

5.2 Vector magnetic data

The X and Z component maps (Figures 13A, 13C) clearly show both the dipolar anomaly associated with the main high-grade ore zone, and the NW-SE fabric revealed in the total field map. The reduced level of detail in Y-component grid (Figure 13B) may be attributed to the orientation of the Y axis along the anomaly strike, leading to smaller signal variation and reduced signal to noise ratio. The line-to-line corrugation observed in the vector component maps is attributed to imperfect attitude correction of the sensor platform. This was attributed mainly to the low sampling frequency of the DGPS system from which sensor azimuth is derived. The resulting corrugation may also be the main cause of the beaded appearance of analytic signal and vertical gradient maps (Figure 12).

In a conventional total field survey it is assumed that the orientation of the field vector remains unchanged, with only the magnitude of the field varying with the proximity to the source. Vector measurements at Deposit #4 demonstrate that the horizontal component of the magnetic field varies dramatically in both direction and magnitude across the site, exceeding 100,000 nT in magnetite-rich areas (Figures 15, 17), with large sharp changes across the main lithology boundaries. For comparison, the horizontal (Y) component of the regional background field is only 4,707 nT (NRCAN, 2014). Due to the high geographic latitude of the study area, the horizontal component of the background geomagnetic field makes up only 8.1% of the observed total field strength, while at mid-latitudes (Hamilton, ON) it amounts to 34.7% (NRCAN, 2014).

One of the objectives of this study was to determine if the RMV and vector attribute maps could provide a basis for distinguishing ore grades, as mineralogic

variations (e.g. transitions between hematite, magnetite and martite) are likely to correspond with changes in magnetic properties. It was shown that residual vector inclination shows a much greater dependence on position relative to the source bodies, as compared to the total magnetic vector. Figure 16A illustrates that the RMV inclination highlights the anomaly shape and feature distribution much better than does the total vector inclination. This demonstrates the advantage of deriving the remanence vector by direct measurement of the vector components, rather than assuming it to be parallel with the induction, as is done during the conventional total field surveys.

Major changes in the magnetic vector orientation coincide with main peaks in total field intensity, as well as with contacts between ore bodies and host rocks (Fig.17). Changes in both inclination and declination occur directly above the inferred zones of specular hematite, magnetite and BIF. In addition, frequency distribution of RMV intensity (Fig. 19C) and vector inclination (Fig. 20C) for the high-grade magnetite are distinct from those of specular hematite and BIF. This shows that combined analysis of the residual vector orientation and RMV intensity can serve as ore body location aide, and mapping of the variations in RMV inclination and declination can be expected to reveal information on the contacts between ore bodies with contrasting remanence directions, as well as to help establish geological contacts (e.g. Ladynin et al., 2002).

However, the low signal-to-noise output of the MEMS accelerometer sensor and the low-frequency nature of the GPS-based azimuth data led to imperfect compensation of the mobile sensor orientation. This allowed walking-induced noise to be introduced into the vector magnetic data, which resulted in the reduced resolution of the final RMV product. Lower-than expected RMV resolution may have prevented identification of potential high-frequency magnetic signatures, unique to various ore grades.

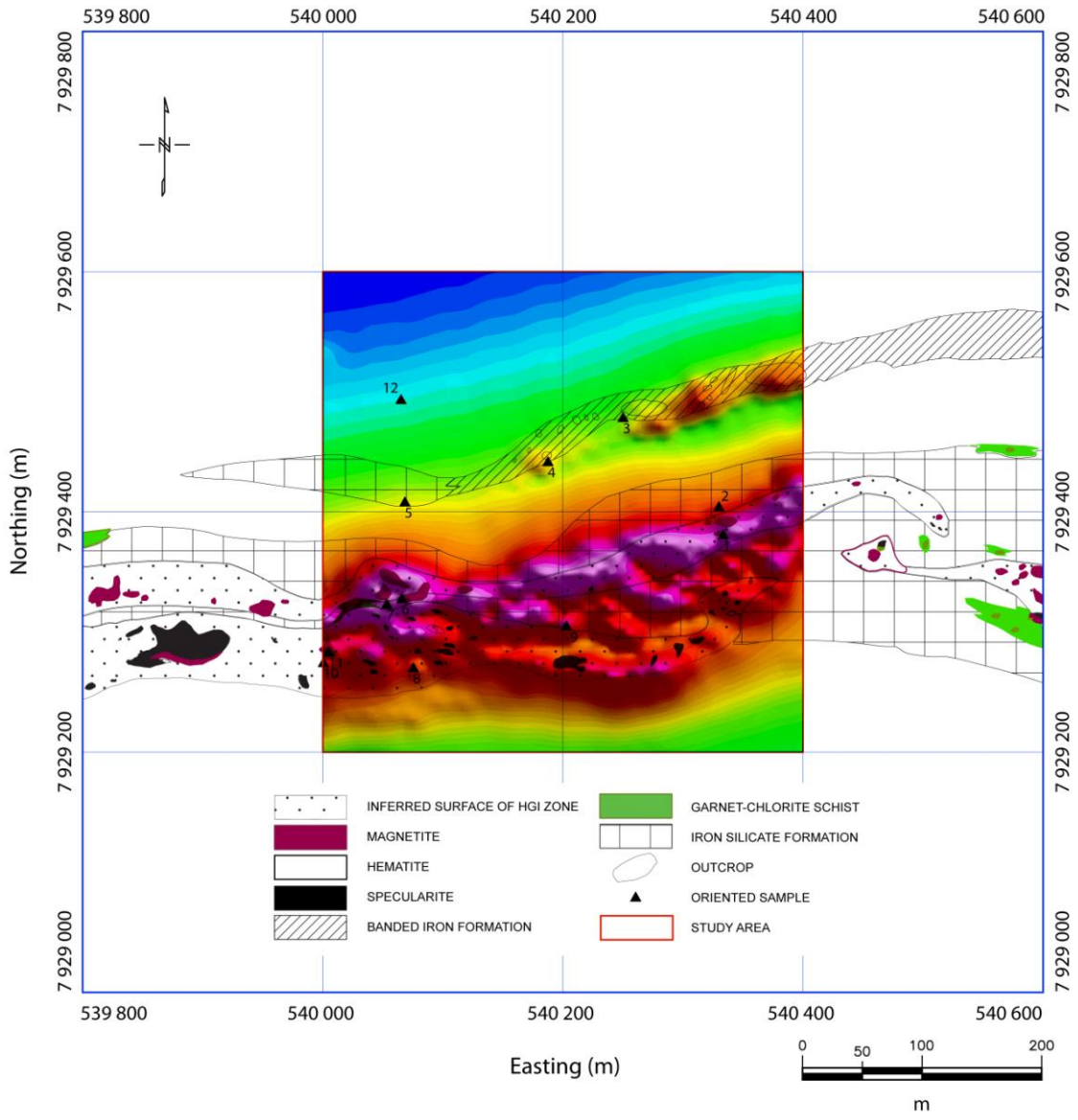

Figure 24. Outcrop geology map overlaid on the RMVI. Note west-east trending zone of high magnetic intensity corresponds closely with inferred belt of high-grade magnetite ore. West-east magnetic high in southern area of map corresponds with a zone of high-grade specularite.

5.3 Vector magnetometer performance

The fluxgate magnetometer system was designed with the objective of acquiring magnetic vector data across high-gradient areas of Deposit #4. The 3-Gauss fluxgate sensor enabled collection of TMI and vector component data across high gradient areas that could not be surveyed using conventional quantum magnetometer systems. The data quality collected by the prototype system, however, suffered from several sources of noise that limited the resolution of the survey data and introduced significant line-to-line levelling problems (e.g. Y-component map Fig. 13B). The most significant source of noise in all component data was uncompensated sensor motion. The sensor motions produced by the movement of the surveyor's pelvis during the walking survey were directly transferred to the sensor boom, causing the sensor to accelerate in a oscillating fashion in addition to being tilted around the pitch and roll axes. The tilt sensor output is a sum of the true and 'apparent' tilt, resulting from lateral acceleration. Tilt sensor output produced by this walking survey can be characterized as high-frequency high-amplitude signal. The high amplitude of the oscillation is attributed to sensor's inability to distinguish between true tilt and lateral acceleration, due to the lack of gyro-compensation. This was confirmed by a simple lab experiment in which the MEMS sensor was placed on a flat table surface, and pushed left-right and then back-forth without any actual tilting. It was observed that side-to-side sliding is interpreted as roll while back-and-forth sliding is interpreted as pitch. The amplitude of the interpreted tilt angle depends on the acceleration during sliding, and reaches large values of up to 30 degrees. This 'apparent tilt' exceeds significantly the magnitude of true tilt angles observed by the surveyor during the field study. As a result, the 'apparent tilt' component can cause a significant error in sensor attitude correction. Subsequent filtering of the magnetic components was necessary as a result, using the low-pass filter implemented in LOWPASS GX extension in Oasis Montaj™ with a cutoff wavelength of 1.5m. This filter algorithm is based on a convolution method developed by Fraser, 1966.

The close correlation between the walking and static survey profiles confirmed the validity of the sensor attitude correction through the use of DGPS and digital accelerometer. While the static survey undoubtedly offered higher measurement accuracy, it was significantly more time-consuming and lacked in down-line resolution. The walking survey required a single day to collect 21 survey lines and 7 tie lines, while collecting measurements for a single static point profile took 2 days.

The sensitivity analysis consisted of two parts: an estimation of the effect of tilt angle on the measured magnetic vector components, as well as measurement of the effect of mechanical oscillation frequency on the accuracy of tilt sensor output. Using the matrix rotation equation, it can be shown that 1° of sensor deviation from horizontal in a vertical ambient field translates into approximately 1,000 nT increase in the X component for each 60,000 nT of total field strength. This increase is measurement error caused by pitch angle deviating from 0°. Similarly, a sensor boom tilted by 2° in a vertical field of 120,000 nT would result in X-component increasing from 0 to 4,188 nT and Z-component decreasing from 120,000 to 119,927 nT. The relative change in the horizontal component is far more dramatic, causing the horizontal component grids to be much more sensitive to errors in pitch and roll correction, as compared to the Z-component. This relationship remains almost linear in the 0-15 degree range, typical for the magnetometer boom swinging range associated with walking. Due to the nature of the sine waveform, the effect of pitch angle on the X component is much greater than that on the Z component in the 0-15 degree range. (See Appendix).

The measured noise in the horizontal component had a consistent wavelength throughout the survey lines, indicating a rhythmic swinging oscillation caused by walking. The noise amplitude appears proportional to the size of observed anomaly. Away from large anomalies, the main noise envelope was +/- 3,300 nT.

6. Summary

A new method for ground-based vector magnetic survey is introduced based on commercially available fluxgate magnetometer, a solid-state digital compass and two D-GPS receivers. In addition to its ability to measure the magnetic vector orientation, the fluxgate magnetometer offered a dramatically enhanced measurement range compared to the conventional Overhauser magnetometers, and permitted mapping of high-grade magnetite ore zones at MRG where the total field intensity was in excess of 380,000 nT. High grade ore zones were identified in RMVI maps by a 15-20 m wide W-E trending zone of high magnetic intensity with a distinctive dipolar signature. A previously unknown northwest-southeast oriented magnetic fabric was defined by linear magnetic lows within the ore zone. Lineaments offsetting the strike of the main high-grade ore zone with an apparent sinistral displacement are interpreted as brittle faults or shear zones. The presence of strong bedding parallel magnetization was indicated by the orientation of the residual magnetic vector.

We have developed and evaluated a method for direct measurement of the residual magnetization vector in extremely high total fields, which was used to reveal new detail in highly-magnetized Mary River high-grade iron ore deposits.

The attitude-corrected walking survey results were validated using a controlled static point vector survey. The obtained RMV inclination highlights the anomaly shape and feature distribution much better than does the total vector inclination. This demonstrates the advantage of deriving the remanence vector by direct measurement of the vector components, rather than assuming it to be parallel with the induction, as is done during the conventional total field surveys. This practical land based vector magnetic survey method can be applied in other exploration projects where magnetic sources may be remanently magnetized.

Acknowledgements

Research work was supported by an NSERC Discovery Grant to J. Boyce and a research grant from Baffinland Iron Mines Corporation (BIMC). I. Inozemtsev was supported in part by a graduate scholarship stipend generously provided by BIMC. We thank BIMC for field logistical support and for access to unpublished reports and geological mapping. We are grateful for technical advice and discussions with industry collaborators Dr. Thomas Iannelli, Ahoora Samiei and Peter Dao. We thank Jeffrey Wannop, Eli Iannelli, Peter Dao and Ludger Makkik for assistance with field work. Magnetic property analyses were conducted by Dr. Bill Morris in the Applied Geophysics lab at McMaster University.

Chapter Three: Conclusions

3.1 Summary

The effectiveness of vector magnetic exploration surveys of strongly remanently magnetized geology was demonstrated by Dransfield et al. (2003) and Isezaski and Matsuo (2009). However, such studies require the use of airborne gravity gradiometer systems with expensive inertial sensors for magnetometer attitude correction. This study evaluated an inexpensive vector magnetometer system for high-resolution ground-based vector magnetic surveys as an alternative to airborne surveys. First in its class, it employed a MEMS accelerometer and dual D-GPS receivers to correct the attitude of a wide-range tri-axial fluxgate magnetometer, eliminating the need for a gyroscope system. High-resolution mapping acquired over Mary River BIF-hosted iron ore deposit in northwestern Baffin Island offered new insights into the complex structure of area, and revealed areas of total field intensity in excess of 380,000 nT. Resulting map products for the first time revealed the full detail on the extent and continuity of the source body and high-grade zones that could not be inferred from previous airborne and ground-based TMI surveys with a sensor range limited to 130,000 nT. A previously unrecognized NW-SE trending fabric was revealed in both total field and vector magnetic maps, which adds new insights into the deformation history the Mary River Group and BIF-hosted ore bodies. We have developed a method for properly measuring the extremely high total field, as well as deriving the residual magnetization map by vector subtraction of the measured magnetic components from the regional geomagnetic field vector. This operation would have been impossible without vector measurements, and using this data a future inversion model can be used to refine the existing geologic model of the deposit.

The residual vector orientation data reveals an inversion in the magnetic vector between the southern and northern sides of the high-grade iron ore source body, with a complex pattern of direction changes throughout magnetite-rich zones. The measured horizontal components of the field greatly exceeded that of the background geomagnetic

field (55,000 nT), highlighting the importance of magnetic vector measurement. Strong bedding parallel magnetization was revealed by the orientation of the residual magnetic vector. This valuable data could not have been obtained from a conventional total field survey.

Paleomagnetic measurements showed a high degree of anisotropy of susceptibility (up to 2.2), confirming strong layer parallel magnetization. Sample testing also revealed high Q ratios for coarse magnetite (5.2) and specularite-hematite ores (30-107) in comparison with host BIF's. The results from Mary River quantify for the first time the significance of remanence and anisotropy effects in BIF-hosted iron ores of the Mary River group. Ellis et al. (2012) demonstrate that remanent magnetization is a significant factor in many recent exploration projects, and it cannot be neglected in magnetic interpretation and inversion modelling of magnetic source bodies. They argue that the fundamentally non-unique nature of potential field inversion makes it possible to produce plausible but flawed solution if non-induced magnetization is not taken into account. As such, any exploration project aiming to model anisotropic source bodies such as BIF's should benefit from a practical vector magnetic survey method, such as one proposed in this study.

The three main iron ore grades found within study area show similar residual vector orientation, suggesting that the remanence may have been acquired around the same time. Analysis of the RMV signal amplitude and peak intensity of the anomalies associated with different ore lithologies reveals distinct magnetic signatures, which may be used for ore grade differentiation.

3.2 Limitations

Two main limitations of the current method are the low sampling frequency of the GPS-base azimuth measurement, and the lack of a reliable syncing mechanism for the three sensors comprising the magnetometer system: DGPS, tilt and fluxgate sensor, which lead to an extended post-processing time. Additional limitation of using a MEMS accelerometer as tilt sensor was the lack of gyro-compensation to help distinguish between lateral acceleration and true tilt.

3.3 Future Work

This study provides an excellent foundation for further development of land-based vector magnetic survey methods. The planned 2015 BIMC exploration program will include ground-based vector magnetic surveys employing a dual-receiver Trimble™ R8 system with a sampling frequency of 10 Hz to improve the accuracy of DGPS-based azimuth correction. A more reliable time-syncing method for data streams is being developed, in order to eliminate phase shifts in platform attitude correction. A three-axis gyro compensated MEMS tilt sensor will be used for tilt measurements. In future work, a Crossbow™ type dual gyro and Inertial Measurement Unit (IMU) can offer additional precision in sensor attitude measurement although the cost may be prohibitive for some survey applications. These improvements will increase in the overall spatial resolution and signal to noise ratio of the vector magnetic survey, allowing better use of source-body location aids such as vertical and total gradient maps.

References

Austin, J., Geuna, S., Clark, D., & Hillan, D., 2014. Remanence, self-demagnetization and their ramifications for magnetic modelling of iron oxide copper-gold deposits: An example from Candelaria, Chile. *Journal of Applied Geophysics*, *109*, 242-255.

Baffinland Iron Mines, 2008. Unpublished Drill Core Logging Codes.

Baffinland Iron Mines, 2011. Unpublished structural sections: Mary River Deposit No.4, boreholes 187, 189, 190.

Baffinland Iron Mines, 2014. Unpublished map: Deposit No.4 and 5 Geology Map compiled and drawn from field data collected in 2010, 2011, and 2014, supplemented with data from G. D. Jackson field notes and maps, 1965; Duke and MacLeod field notes and map, 2009.

Briggs, I.C., 1974. Machine contouring using minimum curvature. *Geophysics*, 39: 39-48.

Bethune, K.M. and Scammell, R.J. (2003b). Distinguishing between Archean and Paleoproterozoic tectonism, and evolution of the Isortoq fault zone, Eqe Bay area, north-central Baffin Island, Canada. Canadian Journal of Earth Sciences, v. 40, p. 1111-1135

Christensen, A. and Dransfield, M., 2002. Airborne Vector Magnetometry over Banded Iron Formations. *SEG Technical Program Expanded Abstracts*, pp. 13-16., *34*, 93-96.

Clark, D.A., 2014. Methods for determining remanent and total magnetisations of magnetic sources – a review. *Exploration Geophysics*, 45, 271-304.

Clark, D. A., & Schmidt, P. W., 1994. Magnetic properties and magnetic signatures of BIFs of the Hamersley Basin and Yilgarn Block, Western Australia. *Exploration Geophysics*, *25*(3), 169-169.

Clark, D. A., Schmidt, P. W., Coward, D. A., & Huddleston, M. P., 1998. Remote determination of magnetic properties and improved drill targeting of magnetic anomaly sources by Differential Vector Magnetometry (DVM). *Exploration Geophysics*, *29*, 312-319.

Dransfield, M., Christensen, A., & Liu, G., 2003. Airborne vector magnetics mapping of remanently magnetized banded iron formations at Rocklea, Western Australia. *Exploration Geophysics, 34*, 93-96.

Edelstein, A. 2007. Advances in magnetometry. *Journal of Physics: Condensed Matter*, 19 165217

Ellis, R.G., de Wet, B. and Macleod I.N., 2012. Inversion of magnetic data for remanent magnetisation direction. *ASEG Extended Abstracts 2012*, 1-4

Ellis, R.G., de Wet, B. and Macleod I.N., 2013. Inversion of magnetic data from remanent and induced sources. *ASEG Extended Abstracts 2013*, 1-4

Gunn, P.J., Dentith, M.C., 1997. Magnetic responses associated with mineral deposits. *Journal of Australian Geology and Geophysics*, 17, 145-178.

Guo,W., Dentith, M., Zhengxiang, L., Powell, C., 1998. Self demagnetization corrections in magnetic modelling: some examples. *Exploration Geophysics*, 29, 396–401.

Hagemann, S., Dalstra, H. I., Hodkiewicz, P., Flis, M., Thorne, W., & McCuaig, C., 2007. Recent advances in BIF-related iron ore models and exploration strategies. In *Proceedings of Exploration* (Vol. 7, pp. 811-821).

Isezaski N., Matsuo J., 2009. Magnetization structure of Aogashima Island using vector magnetic anomalies obtained by a helicopter-borne magnetometer. Exploration Geophysics, 40, 17-26

Jackson, G.D. 2000. Geology of the Clyde-Cockburn Land Map Area, North-Central Baffin Island, Nunavut. Geological Survey of Canada, Memoir 440, 303 p.

Jackson G.D., Berman R.G., 2000. Precambrian metamorphic and tectonic evolution of northern Baffin Island, Nunavut, Canada. *The Canadian Mineralogist*, 38, 399-421.

Jackson, G.D. and Morgan, W.C. 1978. Precambrian metamorphism on Baffin and Bylot island.
In: Metamorphism in the Canadian Shield, (eds.) J.A. Fraser and W.W. Heywood. Geological Survey of Canada, Paper 78-10, pg. 249-267

Johns S.M., Young M.D., 2006. Bedrock geology and economic potential of the Archean Mary River group, northern Baffin Island, Nunavut. Geological Survey of Canada, Current Research 2006-C5, 13p.

Kerr, T. L., O'Sullivan, A. P., Podmore, D. C., Turner, R., & Waters, P., 1994. Geophysics and iron ore exploration: examples from the Jimblebar and Shay Gap-Yarrie regions, Western Australia. *Exploration Geophysics*, *25*, 169-170.

Ladynin A.V., Vasilevski A.N., Pavlov A.F. and Popova A.A., 2002. Vector magnetic surveys in iron prospecting. *Russian Geology and Geophysics*, 43, 1, 75-85

LaValle, S.M. 2006. Planning Algorithms. Cambridge University Press, 842 pp.

Lelièvre P.G., Oldenburg D.W., 2009. 3D total magnetization inversion applicable when significant, complicated remanence is present. Geophysics, 74, 3, 21-30.

Luyendyk, A.P.J., 1997. Processing of airborne magnetic data. *AGSO Journal of Australian Geology & Geophysics*, 17(2): 31-38.

MacLeod I.N., Ellis R.G., 2013. Magnetic vector inversion, a simple approach to the challenge of varying direction of rock magnetization. *In ASEG forum on The Application of Remanent Magnetization and Self-Demagnetisation Estimation to Mineral Exploration, Extended Abstracts*, 41-46.

MacLeod, I.N., Jones, K., and Dai, T.F., 1993. 3-D analytic signal in the interpretation of total magnetic field data at low magnetic latitudes. *Exploration Geophysics*, 24:679-688.

MacLeod M.E., 2012. Metallogenic setting of high-grade iron ores, Mary River District, North Baffin Island, Nunavut. Graduate thesis, University of Western Ontario.

Morris, B., Ugalde, H., & Thomson, V., 2007. Magnetic remanence constraints on magnetic inversion models. *The Leading Edge*, *26*, 960-964.

Mueller, E. L., Morris, W. A., Killeen, P. G., & Balch, S., 1998. Combined 3-D interpretation of airborne, surface, and borehole vector magnetics at the McConnell nickel deposit. *Journal of Environmental and Engineering Geophysics*, *3*, 203-214.

Nabighian, M. N., Grauch, V. J. S., Hansen, R. O., LaFehr, T. R., Li, Y., Peirce, J. W., and Ruder, M. E., 2005. The historical development of the magnetic method in exploration. *Geophysics*, *70*(6), 33ND-61ND.

Natural Resources Canada, Magnetic Field Calculator. Retrieved August 2014. URL: http://geomag.nrcan.gc.ca/calc/mfcal-eng.php

Nelson, B.J., 1994. Levelling total-field aeromagnetic data with measured horizontal gradients. *Geophysics*, 59, 8, 1166-1170.

Paine, J., Haederle, M., & Flis, M., 2001. Using transformed TMI data to invert for remanently magnetised bodies. *Exploration Geophysics*, *32*, 238-242.

Pilkington, M., & Beiki, M., 2013. Mitigating remanent magnetization effects in magnetic data using the normalized source strength. *Geophysics*, *78*, J25-J32.

Pozza, M.R., Boyce, J.I. and Morris, W.A., 2004. Lake-based magnetic mapping of contaminated sediment distribution, Hamilton Harbour, Lake Ontario, Canada. *Journal of Applied Geophysics*, 57, 1, 23-41.

Roest, W.R., Verhoef, J., and Pilkington, M., 1992.Magnetic interpretation usingthe 3-D analytic signal. *Geophysics*, 57, 116-125.

Ripka, P., 2003. Advances in fluxgate sensors. *Sensors and Actuators A: Physical*, *106*, 8-14.

Schmidt, P.W., Clark, D.A., Coward, D.A. and Huddleston, M.P., 1993. Development and application of differential vector magnetometers. *Exploration Geophysics*, 24, 123-126.

Telford, W.M., Sheriff, L.P., 1991. Applied geophysics, second edition. Cambridge University Press, Cambridge. 770 pp.

Ugalde, H., Morris, W. A., Pesonen, L. J., & Danuor, S. K., 2007. The Lake Bosumtwi meteorite impact structure, Ghana—Where is the magnetic source?. *Meteoritics & Planetary Science*, *42*, 867-882.

Wallace, Y., 2007. 3D Modelling of Banded Iron Formation incorporating demagnetisation – a case study at the Musselwhite Mine, Ontario, Canada. *Exploration Geophysics*, 2007, 38, 254-259.

Whiting, T. H., 1986. Aeromagnetics as an aid to geological mapping—a case history from the Arunta Inlier, Northern Territory. *Australian Journal of Earth Sciences*, *33*, 271-286.

Young, M.D, Sandeman, H., Berniolles, F. and Gertzbein, P.M., 2004. A preliminary stratigraphic and structural framework for the Archaean Mary River Group, northern Baffin Island, Nunavut. Geological Survey of Canada, Current Research 2004 C-1, 14 pp.

APPENDIX A: Paleomagnetic analysis results for oriented rock samples

Sample ID	BIM sample ID	Density	LAB Susceptibility				MPP Susceptibility* (SI)	
		g/cc	*10-6 emu/cc	SI	Mean	Std. dev.	Mean	Std. dev.
1-1	3081	4.77	211,568.2	2.6586	2.6243	0.0981	2.5921	0.2888
1-2		4.70	197,185.5	2.4779				
1-3		4.79	213,590.6	2.6841				
1-4		4.75	212,980.5	2.6764				
2-1	3082	2.88	810.8	0.0102	0.0104	0.0003	0.0285	0.0198
2-2		2.89	844.8	0.0106				
3-1	3083	2.98	1,621.8	0.0204	0.0097	0.0073	0.0313	0.0276
3-2		3.46	613.6	0.0077				
3-3		3.38	544.2	0.0068				
3-4		3.43	299.8	0.0038				
4-1	3084	2.92	17,946.7	0.2255	0.2057	0.0625	0.1680	0.1157
4-2		2.47	12,470.8	0.1567				
4-3		2.93	20,448.6	0.2570				
4-4		2.95	18,877.8	0.2372				
4-5		3.08	20,306.3	0.2552				
4-6		2.94	8,155.7	0.1025				
5-1	3085	2.98	1,468.9	0.0185	0.0163	0.0030	0.0081	0.0050
5-2		2.91	1,127.6	0.0142				
6-1	3086	4.63	204,531.4	2.5702	2.5299	0.0570	1.6279	0.3672
6-2		4.60	198,116.5	2.4896				
7-1	3087	4.45	218,523.5	2.7460	2.6208	0.1332	1.5227	0.3473
7-2		4.59	197,426.9	2.4809				
7-3		4.64	209,718.5	2.6354				
8-1	3088	5.17	470.7	0.0059	0.0039	0.0018	0.0056	0.0044
8-2		5.21	211.4	0.0027				
8-3		5.21	252.0	0.0032				
9-1	3089	5.07	226,361.8	2.8445	2.8707	0.0194	2.4606	0.4397
9-2		5.08	228,660.2	2.8734				
9-3		5.07	228,671.9	2.8736				
9-4		5.06	230,089.4	2.8914				
10-1	3090	4.89	202,444.7	2.5440	2.5334	0.0755	2.2689	0.3842
10-2		4.91	207,142.7	2.6030				
10-3		4.89	195,219.3	2.4532				
11-1	3092	5.07	118,864.0	1.4937	1.0219	0.4521	0.1476	0.2010
11-2		5.15	47,153.1	0.5925				
11-3		5.06	77,940.5	0.9794				
12-1	6000	2.68	9.2	0.0001	0.0001	6.73E-06	0.0005	0.0003
12-2		2.69	9.4	0.0001				
12-3		2.69	10.2	0.0001				

Multiples cores were extracted from each sample. First digit indicates sample number. Second digit indicates core.

*Values shown are summary statistics for N=30 readings taken at each outcrop.

Sample ID	Remanence			Q ratio		Anisotropic mag.susc.	
	*10-6 emu/cc	SI	Mean	A95	PEF	%	Max/Min
1-1	16880	0.212	0.2981	12	0.1	11	1.112
1-2	21871	0.275		10	0.2	7	1.071
1-3	25446	0.320		6	0.2	10	1.105
1-4	30676	0.385		8	0.3	9	1.095
2-1	573	0.007	0.0086	7	1.2	32	1.366
2-2	801	0.010		7	1.6	24	1.265
3-1	4072	0.051	0.1020	9	4.4	34	1.408
3-2	9503	0.119		8	26.9 [2]	69	2.117
3-3	7717	0.097		9	24.7 [2]	63	1.944
3-4	11181	0.141		5	64.9 [2]	57	1.867
4-1	1019	0.013	0.0178	10	0.1	48	1.646
4-2	797	0.010		7	0.1	50	1.685
4-3	2040	0.026		7	0.2	31	1.375
4-4	1922	0.024		7	0.2	30	1.354
4-5	1135	0.014		23	0.1	38	1.475
4-6	1566	0.020		15	0.3	33	1.402
5-1	483	0.006	0.0072	9	0.6	78	2.218
5-2	659	0.008		9	1.0	73	2.116
6-1	27693	0.348	0.3475	8	0.2	7	1.077
6-2	27618	0.347		6	0.2	11	1.113
7-1	25043	0.315	0.3680	9	0.2	23	1.261
7-2	44480	0.559		13	0.4	31	1.369
7-3	18326	0.230		9	0.2	22	1.243
8-1	17163	0.216	0.2151	5	63.4 [2]	29	1.340
8-2	17130	0.215		4	140.9 [2]	21	1.241
8-3	17052	0.214		6	117.7 [2]	16	1.178
9-1	868580 [1]	10.915	8.6120	2	6.7 [2]	9	1.054
9-2	973842 [1]	12.238		3	7.4 [2]	2	1.020
9-3	774598 [1]	9.734		13	5.9 [2]	14	1.155
9-4	124257 [1]	1.561		32	0.9	10	1.101
10-1	64122	0.806	1.0698	7	0.6	5	1.056
10-2	35965	0.452		9	0.3	10	1.104
10-3	155317 [1]	1.952		6	1.4	8	1.081
11-1	91020 [1]	1.144	0.5430	6	1.3	37	1.448
11-2	7514	0.094		8	0.3	47	1.599
11-3	31104	0.391		13	0.7	55	1.713
12-1	1	1.4E-5	1.5E-5	27	0.2	17	1.200
12-2	1	1.2E-5		34	0.2	22	1.300
12-3	2	2.1E-5		29	0.3	24	1.182

[1] Remanence values above normal range. Value calculated from instrument modification.
[2] Q Ratio noticeably above 5. Effective vector closely approximates remanence direction after correction for orientation.

Sample ID	Measured remanence vector (Core space)				Corrected remanence vector (Grid North)			
	Core Space		Mean vector		All cores		Mean vector	
	DS	IS	Decl.	Incl.	Decl.	Incl.	Decl.	Incl.
1-1	270	67	339	58	77	53	124	46
1-2	348	44			136	33		
1-3	27	54			164	51		
1-4	324	42			116	28		
2-1	264	38	267	31	169	39	172	32
2-2	269	23			173	24		
3-1	279	70	275	63	92	52	90	45
3-2	262	66			82	49		
3-3	284	67			95	49		
3-4	276	46			89	28		
4-1	93	69	71	65	190	54	190	54
4-2	60	81			297	22		
4-3	67	53			35	22		
4-4	65	57			165	60		
4-5*	43	28	43	28	111	12	111	12
4-6*	114	41	114	41	57	49	57	49
5-1	209	-35	202	-39	174	53	162	54
5-2	194	-43			150	53		
6-1	342	48	342	48	198	25	198	25
6-2	192	79	192	79	145	65	145	65
7-1	165	37	165	37	24	32	24	32
7-2	327	-54	-	-	-	-	-	-
7-3	68	-35	-	-	-	-	-	-
8-1	112	-59	117	-63	227	26	232	25
8-2	115	-62			230	26		
8-3	127	-66			237	26		
9-1	269	-18	258	5	77	7	101	15
9-2	251	16			114	20		
9-3	253	16			114	18		
9-4	138	19			243	38		
10-1	246	18	228	34	-	-	-	-
10-2	203	11						
10-3	245	69						
11-1	264	20	264	27	290	6	316	5
11-2	250	16			287	19		
11-3	283	42			313	-10		
12-1	235	55	270	54	221	7	220	-8
12-2	312	37			218	-47		
12-3	249	54			218	-1		

* Cores drilled into the side of the sample, yielding results different from those drilled into the top.
- Sample fragmented, preventing accurate measurements.

ANISOTROPIC MAGNETIC SUSCEPTIBILITY

Sample ID	MIN					INT					MAX				
	Decl.	Incl.	Susc.	Mean vector		Decl.	Incl.	Susc.	Mean vector		Decl.	Incl.	Susc.	Mean vector	
				Decl.	Incl.				Decl.	Incl.				Decl.	Incl.
1-1	191	14	0.954	193	16	99	10	0.984	99	13	335	73	1.061	330	70
1-2	195	25	0.968	**354**	**20**	95	21	0.995	**253**	**27**	329	56	1.036	**114**	**56**
1-3	184	12	0.956			92	12	0.986			318	73	1.057		
1-4	200	11	0.963			108	9	0.982			340	76	1.055		
2-1	95	38	0.873	73	40	359	8	0.934	149	9	259	51	1.192	255	51
2-2	52	37	0.908	**334**	**39**	149	9	0.940	**52**	**11**	250	51	1.149	**162**	**52**
3-1	26	13	0.842	16	8	127	39	0.973	95	43	281	48	1.185	279	47
3-2	7	2	0.616	**185**	**9**	99	37	1.086	**264**	**61**	274	53	1.305	**92**	**29**
3-3	183	4	0.668	177	11	88	56	1.033			276	34	1.299		
3-4	171	18	0.662	**353**	**15**	68	33	1.103			284	51	1.235		
4-1	168	14	0.743	170	13	261	13	1.035	262	13	33	71	1.222	35	73
4-2	164	15	0.730	**297**	**22**	256	9	1.042	**35**	**22**	15	72	1.230	**165**	**60**
4-3	170	10	0.828			262	12	1.032			43	75	1.138		
4-4	176	11	0.838			269	16	1.030			51	71	1.134		
4-5*	6	11	0.794	9	10	233	75	1.034	243	75	99	11	1.171	101	12
4-6*	11	8	0.833	**129**	**-21**	251	74	1.000	**37**	**-8**	103	13	1.167	**107**	**68**
5-1	290	6	0.637	288	4	193	49	0.948	193	52	25	41	1.414	21	39
5-2	286	2	0.657	**224**	**-18**	193	54	0.951	**304**	**29**	18	36	1.390	**341**	**-54**
6-1	343	31	0.966	205	10	138	57	0.994	50	80	246	12	1.040	116	-4
6-2	165	8	0.962	**39**	**27**	64	53	0.968	**251**	**59**	261	36	1.071	**137**	**14**
7-1	277	6	0.873	277	6	186	10	1.026	186	10	36	78	1.101	36	78
7-2	291	38	0.850	**132**	**2**	46	27	0.987	**41**	**3**	161	39	1.163	**253**	**86**
7-3	329	8	0.893			226	60	0.998			64	29	1.109		
8-1	161	70	0.841	156	43	318	19	1.031	347	47	51	7	1.127	254	18
8-2	148	32	0.878	**70**	**42**	345	57	1.039	**81**	**-47**	243	8	1.089	**358**	**-9**
8-3	161	26	0.920			35	50	0.996			266	28	1.084		
9-1	353	25	0.949	344	33	97	28	0.986	88	22	228	51	1.000	206	50
9-2	321	62	0.991	**151**	**-59**	149	28	1.002	**253**	**-8**	57	3	1.012	**168**	**29**
9-3	336	37	0.919			81	19	1.019			193	47	1.062		
9-4	343	35	0.948			87	19	1.008			200	48	1.044		
10-1	171	16	0.966	-	-	265	13	1.014	-	-	34	69	1.020	-	-
10-2	357	27	0.947	-	-	109	37	1.007	-	-	240	41	1.045	-	-
10-3	194	61	0.958	-	-	306	11	1.007	-	-	41	26	1.036	-	-
11-1	197	39	0.822	201	32	84	26	0.989	85	35	329	41	1.189	320	39
11-2	213	23	0.783	**349**	**52**	99	44	0.965	**74**	**-4**	322	37	1.252	**341**	**-37**
11-3	191	32	0.766			75	35	0.923			310	39	1.312		
12-1	92	1	0.909	280	63	182	28	1.000	142	15	0	62	1.091	22	29
12-2	263	62	0.833	**230**	**-9**	142	15	1.000	**312**	**67**	45	21	1.083	**301**	**-40**
12-3	280	0	0.917			190	89	1.000			10	1	1.083		

* Cores drilled into the side of the sample, yielding results different from those drilled into the top

- Sample fragmented, preventing accurate measurements.

Mean vector orientation column shows both core space (plain type) and grid-north corrected values (bold).

APPENDIX B: Magnetic interference tests

Magnetic interference tests were performed in order to measure the magnetic anomalies created by the DGPS receiver and console. Magnetic field intensity was measured using the Fluxgate magnetometer, as separation distance between the sensor and DGPS components was increased from 0.2m to 1.2m in 0.1m increments. A 20-second average and standard deviation were recorded at each separation step.

The anomaly generated by the DGPS antenna displays does not follow the anticipated exponential decay with distance, suggesting that it may consist mainly of the instrument background noise. The noise envelope of +/-20 nT was also measured during a 30-minute background test. During the survey, the DGPS antenna was located at a distance of 0.7m, and console at 1.1m from fluxgate sensor.

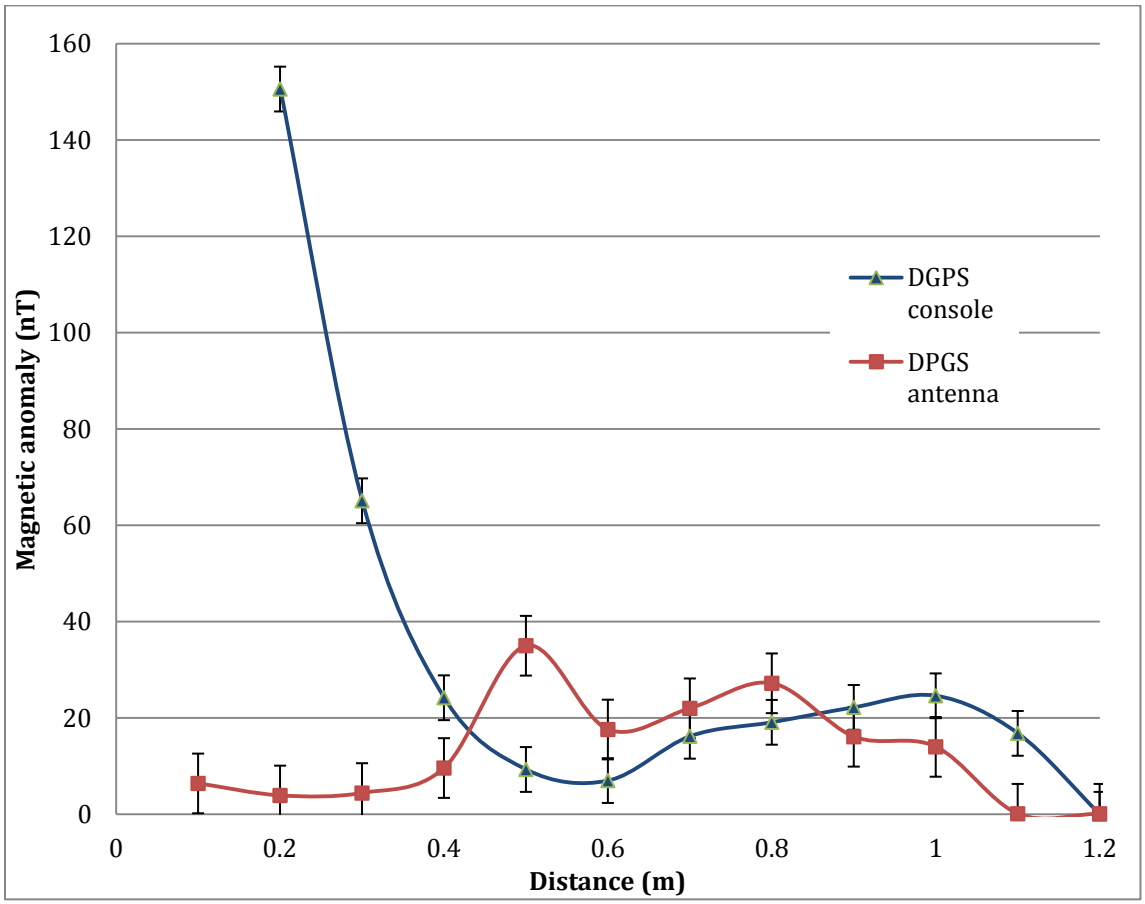

APPENDIX C: Sensor tilt and its effect on horizontal component measurement

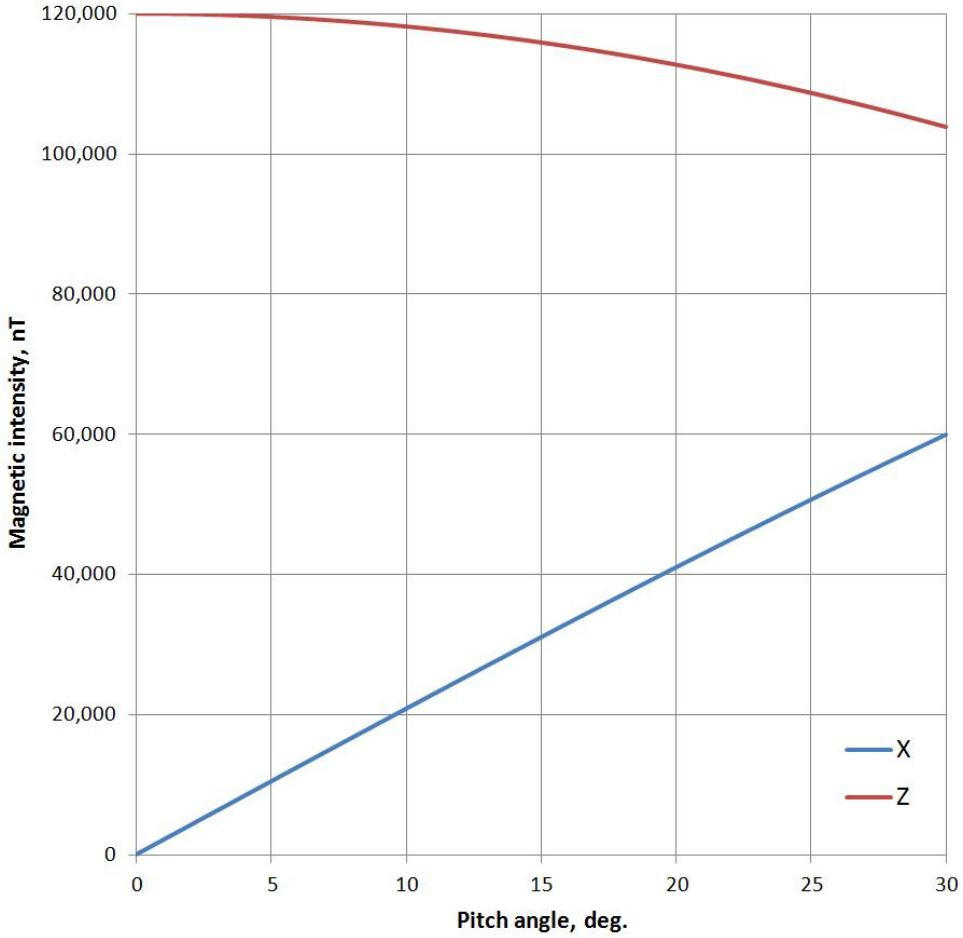

Figure A-2. Effect of the angle of sensor pitch from horizontal on the changes in measured X and Z components of the magnetic field vector, in a vertical ambient field with a total intensity of 120,000 nT. In this simplified example Y component is assumed to be zero, and X and Z components are related as follows: $TMI = \sqrt{X^2 + Z^2}$. At low angles of pitch (<30°), the relative change in X is much greater than the change in Z for a given change in pitch. The roll angle has the same effect on relationship between Y and Z components. This illustrates the need for accuracy in measuring pitch and roll angles.

APPENDIX D: Characteristic profiles of sensor platform attitude angles

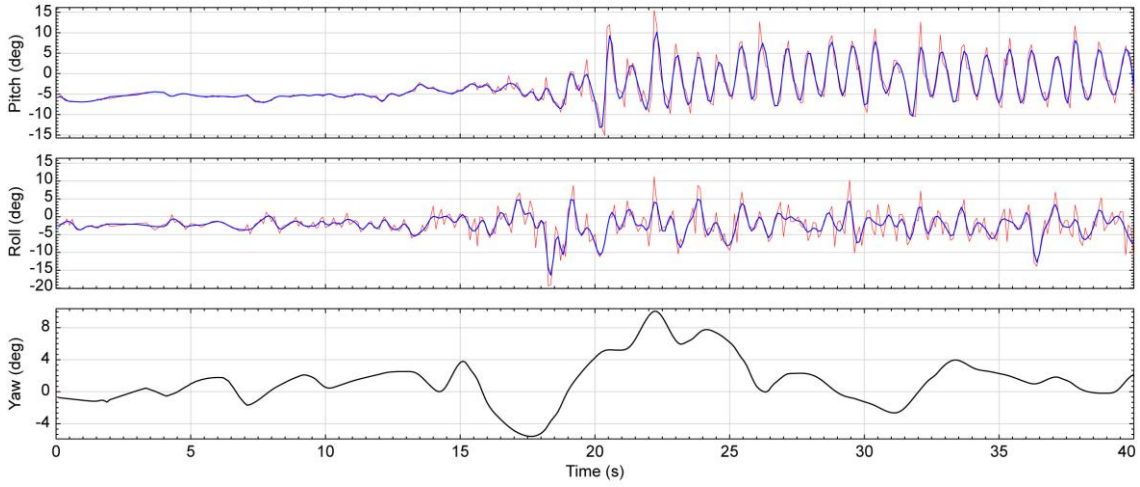

Figure A-3. Characteristic profiles of pitch, roll and yaw angles used for sensor attitude correction. Pitch and roll were measured with a MEMS accelerometer sampling at 13 Hz, and required low-pass filtering to smooth the profile, using the method of Fraser, 1966. The LOWPASS routine in Oasis Montaj with a 5-sample filter window was determined to provide the best smoothing while retaining the original oscillation frequency, and is shown in blue on the profiles. Yaw angle was derived using two D-GPS receivers sampling at 1 Hz, and was interpolated using the minimum curvature method in Oasis Montaj (INTERP GX).

APPENDIX E: Static point vector magnetic measurements at sample sites

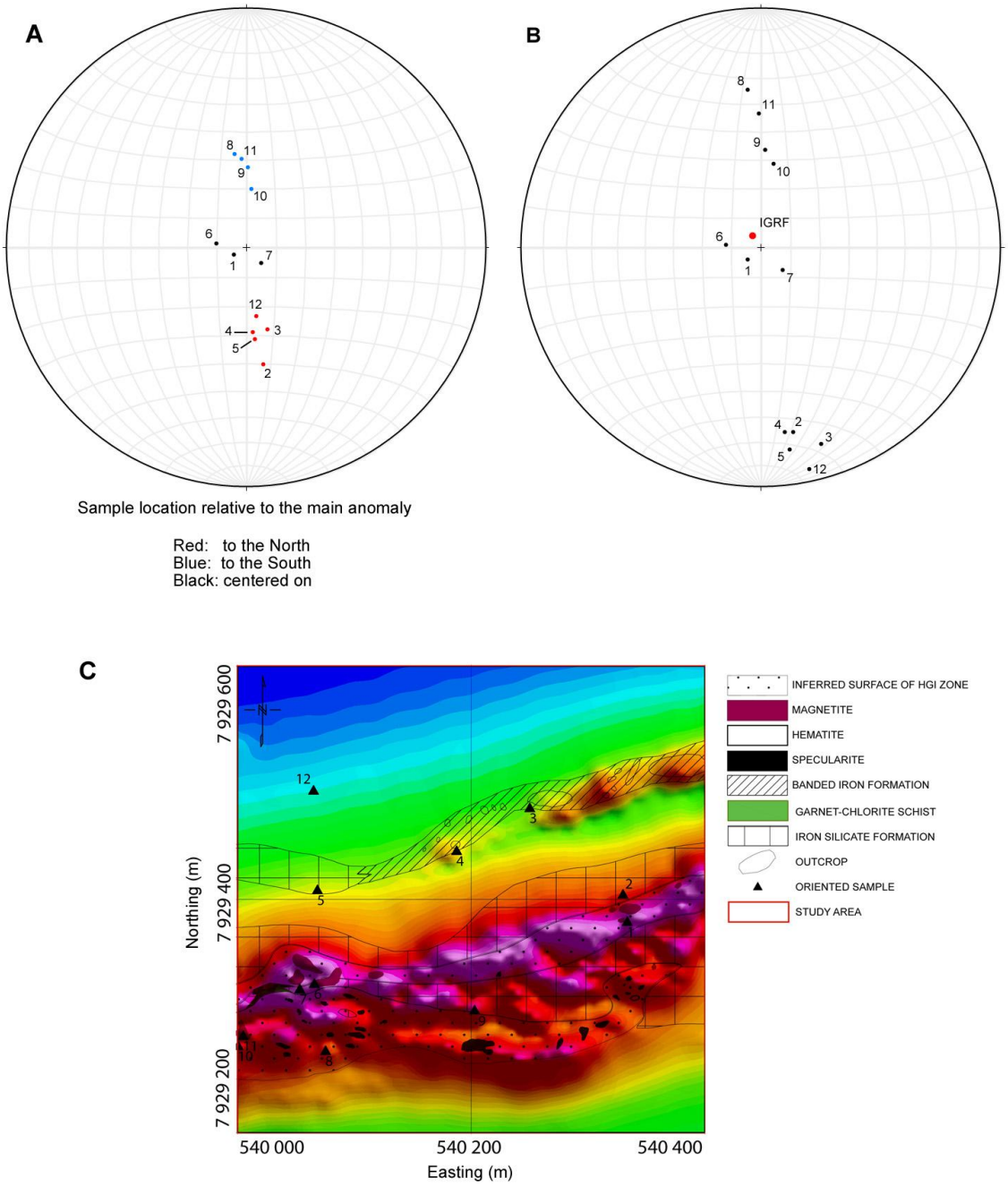

Figure A-4. Static magnetic vector orientation at sample sites, measured directly above paleomagnetic samples, approximately 1m above surface. A) Total magnetic vector (TMV). B) Residual Magnetic Vector (RMV). C) Sample locations relative to magnetic anomaly, and outcrop geology map.